Porkoláb, K., Willingshofer, E., Sokoutis, D., Creton, I., Kostopoulos, D., Wijbrans, J. (2019): Cretaceous-Paleogene tectonics of the Pelagonian zone: inferences from Skopelos island (Greece). - *Tectonics*, *38*, 6, pp. 1946—1973.

DOI: http://doi.org/10.1029/2018TC005331

Tectonics

RESEARCH ARTICLE
10.1029/2018TC005331

Special Section:
Geodynamics, Crustal and Lithospheric Tectonics, and active deformation in the Mediterranean Regions (A tribute to Prof. Renato Funiciello)

Cretaceous-Paleogene Tectonics of the Pelagonian Zone: Inferences From Skopelos Island (Greece)

Kristóf Porkoláb[1], Ernst Willingshofer[1], Dimitrios Sokoutis[1], Iverna Creton[1,2], Dimitrios Kostopoulos[3], and Jan Wijbrans[4]

[1]Faculty of Geosciences, Utrecht University, Utrecht, Netherlands, [2]Now at GFZ Potsdam, Potsdam, Germany, [3]Faculty of Geology and Geoenvironment, National and Kapodistrian University of Athens, Athens, Greece, [4]Faculty of Earth and Life Sciences, VU University Amsterdam, Amsterdam, Netherlands

Abstract We have investigated subduction-exhumation processes in the Pelagonian zone, exposed on the Northern Sporades islands (Aegean Sea) related to successive episodes of ocean continent and continent-continent convergence through integrating multiscale structural analysis, metamorphic petrology, and white mica $^{40}Ar/^{39}Ar$ dating. Two major progressive phases of ductile deformation are documented, which are related to distinct episodes of tectonic burial and exhumation of the Pelagonian continental margin, which was facing the Neotethys/Vardar ocean. Review of existing data sets from neighboring regions shows that both deformation phases can be correlated along strike up to the Dinarides. The first phase of tectonic burial and exhumation (D1) is characterized by NW-SE tectonic transport, greenschist facies metamorphism, and Early Cretaceous (~105-135Ma) $^{40}Ar/^{39}$ Ar white mica single fusion ages. D1 is correlated with the initial closure of the Vardar ocean by top-to-the-W to NW ophiolite obduction and the underthrusting of the Pelagonian margin below the oceanic upper plate. Underthrusting was followed by exhumation and the deposition of Late Cretaceous-Paleogene sediments. The second phase of burial and exhumation (D2) is characterized by NE-SW tectonic transport, greenschist to blueschist facies metamorphism, and latest Cretaceous-Early Eocene $^{40}Ar/^{39}$ Ar white mica ages of S_2 fabrics. Top-to-the-SW shearing is correlated with the tectonic burial of the Pelagonian zone below the Eurasian continent (Rhodopia), while top-to-the-NE shearing is attributed to subsequent extensional exhumation. D2 fabrics record low-grade *P-T* conditions suggesting that the decoupled cover formations exposed on Skopelos were incorporated in an accretionary wedge that formed above the subducting Pelagonian basement during Paleogene times.

Key Points:
- Investigation of successive burial-exhumation cycles by structural analysis and $^{40}Ar/^{39}Ar$ dating
- Early Cretaceous deformation and metamorphism are linked to the underthrusting of the Pelagonian margin below the Vardar ophiolites
- Paleogene deformation and metamorphism of Skopelos are governed by accretionary wedge evolution between Pelagonia and Rhodopia

Correspondence to:
K. Porkoláb,
k.porkolab@uu.nl

Citation:
Porkoláb, K., Willingshofer, E., Sokoutis, D., Creton, I., Kostopoulos, D., & Wijbrans, J. (2019). Cretaceous-Paleogene tectonics of the Pelagonian zone: Inferences from Skopelos island (Greece). *Tectonics*, *38*, 1946–1973. https://doi.org/10.1029/2018TC005331

Received 18 SEP 2018
Accepted 3 MAY 2019
Accepted article online 21 MAY 2019
Published online 19 JUN 2019

1. Introduction

Successive episodes of continent-ocean and continent-continent convergence may result in the repeated tectonic burial and exhumation of a continent or continental block and lead to a complex polyphase deformation history recorded by metamorphic rocks. The Aegean region (Figure 1) provides an opportunity to investigate such a succession of events, since episodes of oceanic and continental subduction, obduction, and continent-continent collision have all taken place during the alpine evolution of the region (Bortolotti et al., 2013; Brun et al., 2016; Goffé et al., 1988; Jolivet & Brun, 2010; Maffione et al., 2015; Robertson, 2004; Schmid et al., 2008). The complexity of the Aegean evolution requires an integrated approach: it has been demonstrated that studies which couple structural analyses with petrological and/or geochronological investigations can significantly contribute to the understanding of regional geodynamics (e.g., Laurent et al., 2017; Lips et al., 1998, 1999; Philippon et al., 2011; Walcott, 1998).

The Pelagonian zone in Greece (Figure 1) records multiple phases of deformation and metamorphism related to continent-ocean and subsequent continent-continent convergence (Kilias et al., 2010; Lips et al., 1998; Most, 2003; Schenker et al., 2014; Schermer et al., 1990; Sharp & Robertson, 2006; Walcott, 1998). Obduction of Jurassic ophiolites from the Neotethys ocean in the Late Jurassic-Early Cretaceous was followed by the collision between Pelagonia and Rhodopia and the subsequent subduction of Pelagonia below Rhodopia in the latest Cretaceous-Paleogene (e.g., Ricou et al., 1998; Schermer et al., 1990; Sharp & Robertson, 2006; Spray et al., 1984). The repeated burial was followed by extensional exhumation adding further to the complexity of the superimposed deformation phases (Brun et al., 2016; Jolivet & Brun, 2010; Walcott, 1998). Consequently, the Pelagonian zone offers many open questions especially regarding the

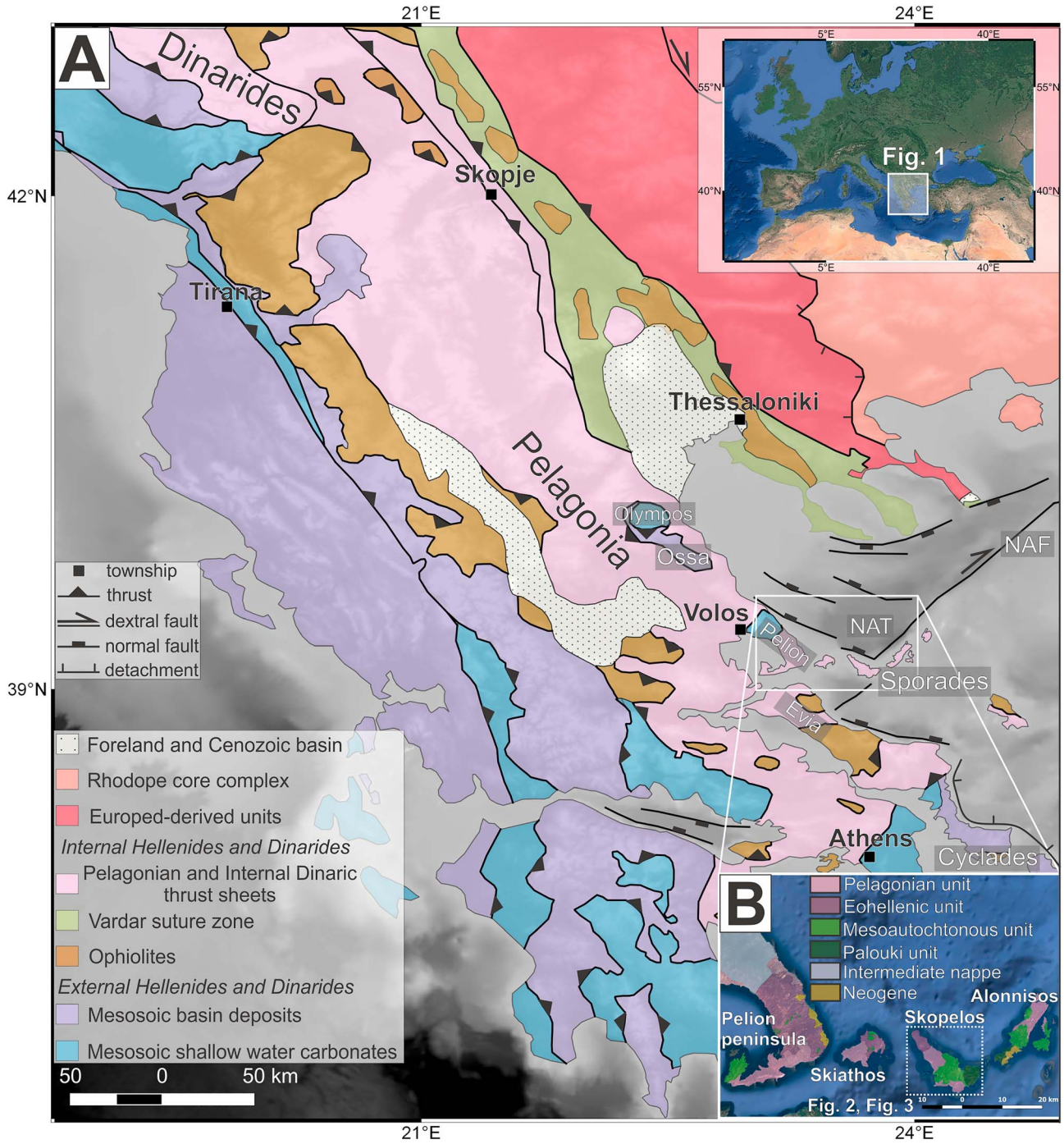

Figure 1. (a) Simplified geological map of the Aegean domain showing the main tectonic units and important structures (modified after Burg, 2012). The greyscale background elevation map is based on GMRT data (Ryan et al., 2009). NAF=North Anatolian fault; NAT=North Aegean trough. (b) Map showing the main geological units of the Northern Sporades and the Pelion peninsula following the subdivision of Jacobshagen et al. (1978) Location of Figure 1b is shown by white bracket.

definition of structural units, tectonic transport directions, and the timing and metamorphic grade of deformation events.

In this study, we have investigated the geological record of tectonic burial and exhumation in the eastern part of the Pelagonian zone (Figure 1), exposed on the Northern Sporades, an island group in the northern Aegean region.

In particular, we present a field-based study from the island of Skopelos that integrates structural and petrological analyses with white mica $^{40}Ar/^{39}Ar$ dating in order to delineate phases of tectonic burial and exhumation and to determine their timing, kinematics, and metamorphic conditions. Comparison of our new data with published data sets allows for discriminating between burial-exhumation related to obduction tectonics, and burial-exhumation related to the Pelagonia-Rhodopia collision as well as for correlating deformation events within the Pelagonian zone at large scale. We conclude with discussing our new results in the frame of Cretaceous-Paleogene geodynamic processes within the Aegean realm.

2. Geological Setting

2.1. Mesozoic-Paleogene Geological Evolution of the Pelagonian Zone

The Pelagonian is defined as a NW-SE trending zone in the Republic of North Macedonia and Greece consisting of thrust sheets that record Alpine orogenic events (Aubouin et al., 1976) and is bordered by the Neotethys/Vardar oceanic suture zone in the NE and the external Hellenides (Pindos and Adria) in the SW (Figure 1a). The Pelagonian zone is either interpreted as an Adria-derived tectonic unit representing the passive margin that was facing a single Neotethys ocean (e.g., Bortolotti et al., 2005; Mercier et al., 1975; Schmid et al., 2008) or as a microcontinent separated from Adria by the Pindos and from Eurasia by the Vardar oceans (e.g., Dilek et al., 2007; Robertson et al., 1996; Sharp & Robertson, 2006). Late Paleozoic-Early Triassic rifting during the break-up of Pangea and subsequent Early-Middle Triassic spreading led to the formation of a passive margin facing the Neotethys/Vardar ocean within the Pelagonian realm (e.g., Bortolotti & Principi, 2005; Stampfli & Borel, 2002). Rifting and marine invasion was reflected in the deposition of Permian and Early Triassic synrift and postrift sediments on top of the Variscan basement, and extensive deposition of carbonate platform sediments from Middle Triassic to Middle Jurassic times (e.g., De Bono, 1998; De Bono et al., 2001; Scherreiks et al., 2010). Upper Paleozoic-Early Triassic (meta)clastic deposits together with thick Pelagonian carbonates of Triassic and Jurassic age characterize a significant part of the Pelagonian zone, including the Sporades and the Pelion peninsula (Figure 1b). Deep water sediments and volcanic-sedimentary mélange successions of similar age are found in the same area (Jacobshagen & Wallbrecher, 1984; De Bono, 1998; Sharp & Robertson, 2006). A similar volcanic-sedimentary succession on the Sporades called the "Eohellenic unit" consists of clastic metasediments, thin-bedded marbles, and mafic metavolcanics of unknown stratigraphic range (Jacobshagen et al., 1978; Jacobshagen & Matarangas, 2004; Jacobshagen & Wallbrecher, 1984; Matarangas, 1992). The Pelagonian carbonate platforms drowned in the Middle-Late Jurassic as marked by deposits of reef debris carbonates intercalated with nodular cherty carbonates. Late Jurassic radiolarites and greywackes are found in the upper members of the deepening sequence (Danelian & Robertson, 2001; Robertson, 1991; Scherreiks, 2000).

The Permian-Jurassic sedimentary succession of the Pelagonian zone is overlain by obducted ophiolitic rocks that originated in the Neotethys ocean. The ophiolites probably formed in a suprasubduction zone setting following intraoceanic subduction initiation (Barth et al., 2008; Clift & Dixon, 1998; Maffione et al., 2015). Middle-Late Jurassic radiometric ages of the metamorphic sole at the base of the ophiolitic nappe attest to the early phases of intraoceanic obduction (Bortolotti et al., 2013; Clift & Dixon, 1998; Dilek et al., 2007; Dimo-Lahitte et al., 2001; Liati et al., 2004; Maffione et al., 2015; Robertson, 2004). Intraoceanic obduction was followed by the emplacement of the ophiolitic thrust sheet(s) onto the Pelagonian passive margin leading to deformation and metamorphism in the Pelagonian zone. This Late Jurassic-Early Cretaceous tectono-metamorphic event of various metamorphic grade (greenschist facies to partial melting) has been reported from various locations along the Pelagonian zone as well as in the Dinarides providing evidence for the tectonic burial of the passive margin following ophiolite obduction (e.g., Kilias et al., 2010; Lips et al., 1999; Most, 2003; Schefer, 2012; Schenker et al., 2014; Schermer et al., 1990; Schmid et al., 2008; Sharp & Robertson, 2006; Tomljenović et al., 2008; Walcott, 1998).

The burial of the Pelagonian margin was followed by exhumation and the formation of a regional Late Jurassic-Early Cretaceous erosional unconformity in the Evia-Pelion-Sporades region (Jacobshagen & Wallbrecher, 1984; De Bono, 1998). Karstification of the Pelagonian carbonates was associated with the

accumulation of bauxites and laterites (e.g., Jacobshagen & Wallbrecher, 1984; Robertson, 1991). Deposition of Albian-Turonian transgressive conglomerates, carbonates, and finally Turonian-Paleogene flysch marks Late Cretaceous transgression and the evolution of a foredeep, which in all likelihood marks the final closure of the Neotethys/Vardar ocean between Pelagonia and Eurasia (Jacobshagen & Wallbrecher, 1984). This Upper Cretaceous-Paleogene sedimentary sequence is referred to as Mesoautochtonous unit (Jacobshagen & Wallbrecher, 1984). A stratigraphically similar but structurally distinct succession is called the Palouki unit which crops out on Skopelos and Alonnisos (Figure 1b). The Mesoautochtonous and the Palouki unit have experienced low-grade metamorphism and intense deformation due to the final closure of the Neotethys ocean and following nappe stacking, which is assumed to be of Eocene in age based on the age of the Flysch formations (Jacobshagen & Wallbrecher, 1984; Matarangas, 1992). Similar tectono-metamorphic events ranging from Late Cretaceous to Late Paleogene in time and greenschist to blueschist facies metamorphism have been reported from many locations within the Pelagonian zone (e.g., Lips et al., 1999; Schermer et al., 1990; Walcott, 1998) and also from the more external domains of the Hellenides like the Cyclades (e.g., Altherr et al., 1979; Blake et al., 1981; Bröcker et al., 1993; Lister & Forster, 2016; Wijbrans et al., 1990). Final closure of the Neotethys/Vardar ocean resulted in regional nappe stacking and the formation of the generally SW-verging Hellenides (Figure 1a) with metamorphic rocks in the lower tectonic units like Pelagonia, Pindos, and Adria experiencing largely top-to-the-SW sense of shear (Brun et al., 2016; Jolivet & Brun, 2010). Subduction of continental crust such as Pelagonia might have contributed significantly to the initiation of slab-rollback (Brun & Faccenna, 2008), which has controlled upper plate extension and exhumation in the Aegean by detachment systems with mainly top-to-the-NE kinematics since Paleogene times (Brun et al., 2016; Brun & Sokoutis, 2007; Gautier & Brun, 1994).

2.2. Geology of Skopelos

The island of Skopelos belongs to the Northern Sporades, a group of islands located approximately 100 km north of Athens, due east of Volos and which are part of the Pelagonian zone. In the following paragraphs, we will describe the structure and stratigraphy of Skopelos island from bottom to top, following the subdivision of Matarangas (1992). The lowermost unit is the Pelagonian, which consists of Upper Paleozoic-Carnian mixed metaclastic-carbonate (thin-bedded marble) succession and conformably overlying Carnian-Jurassic (?) thick-bedded carbonates (marbles and dolomites; Matarangas, 1992). Jurassic carbonates in the Pelagonian unit have been reported from the neighboring island of Alonnisos (Figure 1b; Kelepertsis, 1974); however, these observations have not been confirmed from Skopelos yet. The Glossa unit structurally overlies the Pelagonian unit (Matarangas, 1992). It is mainly a metasedimentary-metavolcanic succession consisting of phyllites, metasandstones, thin-bedded marbles that contains slices of metabasalts and Cipolines (pale green marbles with tuff content; Matarangas, 1992). The stratigraphic age of the Glossa unit is uncertain as is its provenance. This unit has been interpreted as part of the Pelagonian unit based on lithological similarities (Jacobshagen et al., 1978), or as part of the Eohellenic nappe, which represents the transition from the distal Pelagonian margin toward the Neotethys/Vardar ocean (Jacobshagen & Matarangas, 2004; Matarangas, 1992). The latter interpretation implies that the Glossa and the Pelagonian units on Skopelos are time equivalents (Upper Paleozoic-Jurassic). According to Matarangas (1992), the Glossa unit has been thrust on top of the Pelagonian probably in Early Cretaceous times when the Jurassic ophiolites of the Neotethys ocean were emplaced on top of the Pelagonian zone. Both the Pelagonian and the Glossa units record low-grade metamorphism and pervasive folding (Matarangas, 1992).

The Pelagonian and Glossa units are truncated by an erosional unconformity, which forms the base of the younger sedimentary cycle, the Mesoautochtonous unit. The unconformity is marked by metabauxites and Al-rich metapelites, which mainly fill the uneven karstified surface of the Pelagonian dolomites on Skopelos (Figure 2) as well as the Glossa unit on Skiathos (Figure 1b). Petrological analysis of the Al-rich metapelites has shown the occurrence of carpholite and chloritoid, which implies high-pressure metamorphic conditions (Mposkos & Liati, 1991). The metabauxites and metapelites are considered to be of Albian age (Matarangas, 1992); however, different Late Jurassic-Early Cretaceous ages cannot be ruled out due to the time range of the regional hiatus (e.g., Robertson, 1991). On top of the metabauxites-metapelites, Albian-Cenomanian transgressive conglomerates occur, which are gradually pass to

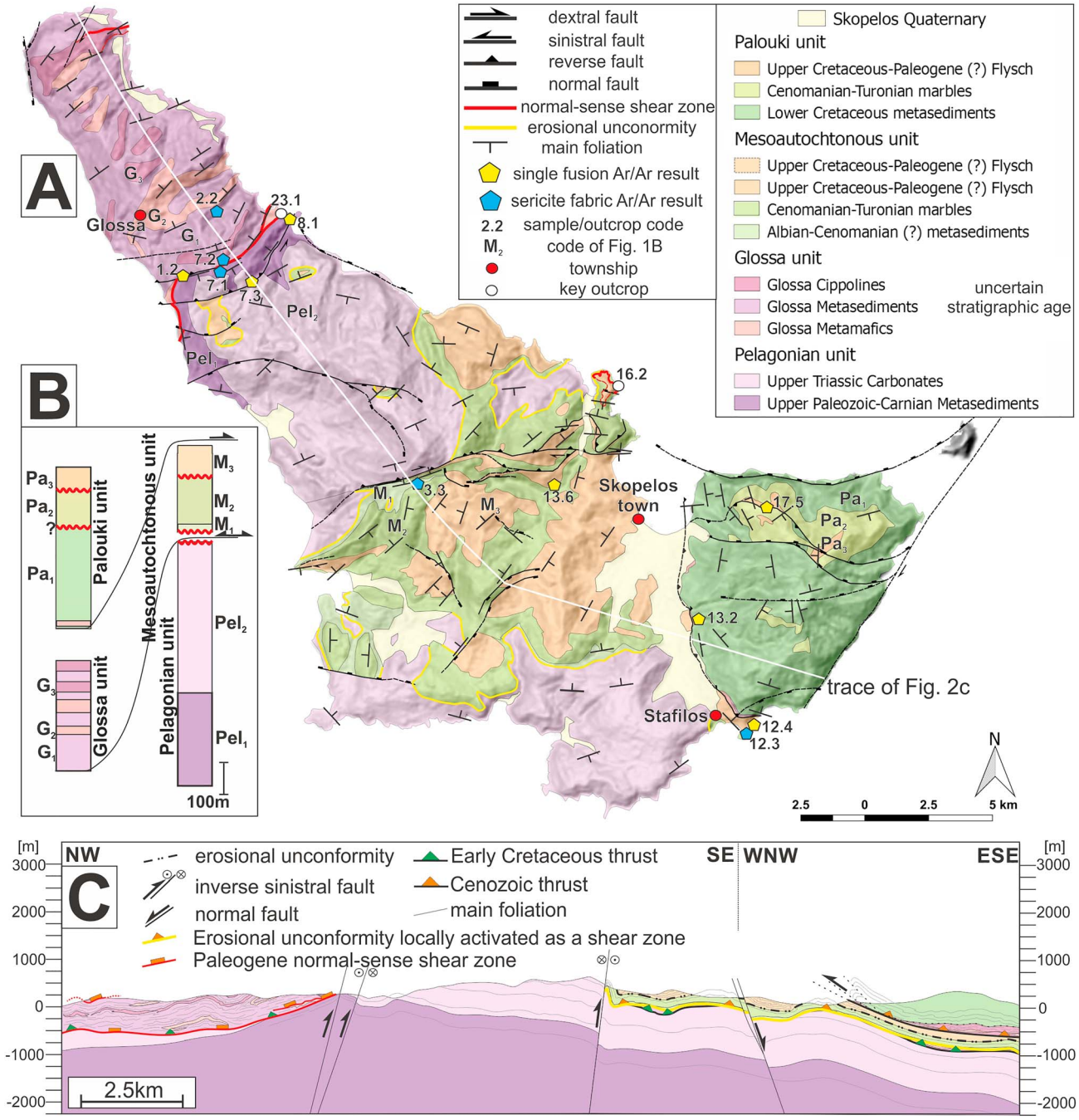

Figure 2. (a) Geological map of Skopelos (modified after Matarangas, 1992) showing the major structures, measurements of the main foliation, and important locations on the island. (b) Tectonostratigraphic column showing the approximate outcropping thickness of the formations. (c) Cross section through Skopelos island. Trace of the cross section is shown on Figure 2a by white line.

Cenomanian-Turonian carbonates. The carbonates exhibit well-foliated, rudist-bearing marbles as well as massive dolomitic layers with barely visible foliation. The carbonates are unconformably overlain by a largely fine-grained metaclastic succession, the Mesoautochtonous Flysch unit. The age of the flysch was described as Maastrichtian-Paleogene (Matarangas, 1992). Fossils found in the flysch confirm the extent of this formation into the Paleocene and possibly into the Eocene (Matarangas, 1992). The entire Mesoautochtonous sequence experienced low-grade metamorphism and pervasive deformation (Jacobshagen & Wallbrecher, 1984; Matarangas, 1992).

Skopelos exhibits another tectonic unit with similar Cretaceous strata: the Palouki unit (Figures 1b and 2). This unit lies on top of the Mesoautochtonous unit separated by a thrust (Figure 2). It consists of three formations. The upper two formations are equivalents of the marbles and the overlying flysch of the Mesoautochtonous unit; they share lithological and stratigraphic characteristics (Cenomanian-Turonian marbles and Upper Cretaceous-Paleogene flysch; Matarangas, 1992). In contrast, the lowest and thickest formation of the Palouki unit is uncertain in age and is lacking equivalents in the region. It largely consists of fine-to medium-grained metaclastic sediments and thin-bedded marbles. Based on the lithofacies, a deep-water origin was proposed for the lowest Palouki formation (Matarangas, 1992). Its contact with the overlying Cenomanian-Turonian carbonates is uncertain; it could either be conformable or erosional (Matarangas, 1992). The base of the formation and thus of the whole Palouki unit exposes mafic volcanic bodies, fine-grained dark phyllites, and serpentinite blocks. Based on these findings, it was assumed that the Palouki unit was deposited on the Eohellenic nappe (Glossa unit on Skopelos; Matarangas, 1992). Fossils are scarce and document an Upper Jurassic-Lower Cretaceous stratigraphic range (Matarangas, 1992). The Palouki nappe experienced low-grade metamorphism and pervasive deformation similar to the Mesoautochtonous unit (Matarangas, 1992).

3. Analytical Methods

3.1. Microprobe Analyses for Pressure-Temperature Calculations

Microprobe analyses were performed in order to constrain the chemical composition and gain the input for thermodynamic calculations of a prospective shear zone (outcrop 3.3 on Figure 2a). The microprobe analyses were conducted at the Department of Geological Sciences, School of Mining and Metallurgical Engineering, National Technical University of Athens, Greece, using a JEOL JSM-6380LV scanning electron microscope equipped with an EDS Oxford Instruments INCA 505 analytical system. Operating conditions were accelerating voltage 20 kV, beam diameter 1 μm, probe current 20 nA, and counting time 80 s. Standards used were wollastonite (Si, Ca), rutile (Ti), corundum (Al), hematite (Fe), rhodonite (Mn), periclase (Mg), jadeite (Na), and orthoclase (K). Results of the analyses are listed in Table A1, and the P-T estimations based on the results are given in section 4.3.

3.2. $^{40}Ar/^{39}Ar$ Dating

$^{40}Ar/^{39}Ar$ dating of white micas was performed with the objective to link deformation phases recorded by the metamorphic rocks exposed on Skopelos with thermal and/or crystallization events. It has been demonstrated that conventional multigrain step heating $^{40}Ar/^{39}Ar$ dating of mixtures of white micas (Schermer et al., 1990) as commonly occur in the blueschist-greenschist domain may result in geologically meaningless age spectra without knowing the precise end-members of the mixture (Bröcker et al., 2013; Lister & Forster, 2016). Warren et al. (2012) made the point that under such PT conditions muscovites or phengites may yield crystallization ages meaning that resetting is not achieved by thermally activated diffusion. To avoid difficulties in interpretation and gain the maximum information from our samples, we applied two ways of $^{40}Ar/^{39}Ar$ dating: (1) determination of the $^{40}Ar/^{39}Ar$ age of fine-grained mylonitic foliations by step heating experiments on fine-grained sericite fabrics (S_2 on Figures 5b–5e) and (2) determination of the $^{40}Ar/^{39}Ar$ age of larger (≥250μm) white mica crystals with the multiple single-grain fusion dating method (Figures 5a and 5f). The applicability of white mica $^{40}Ar/^{39}Ar$ fabric and single-grain fusion dating approach for the detection of multiple tectonic events has been proven by several works as well as that careful microstructural characterization of the samples allows for selective dating of different foliations (Beltrando et al., 2009; Lips et al., 1998; Lister & Forster, 2016; Uunk et al., 2018; Wijbrans et al., 1990). Thus, by the combined usage of fabric and single-grain fusion methods we may expect to gain time constraints for multiple main stages of ductile deformation on Skopelos. A short description of the dated samples is given in Table A3.

In case of the fine-grained sericite fabrics we used groundmass separates because individual sericite grains were too small for separation. The grain size of the groundmass separates was 250–500 μm. The methodology of ground mass dating followed Pascual et al. (2013).

For the purpose of single-grain fusion dating white mica crystals of the crushed samples were separated from 250- to 500-μm sieve fractions using a Faul vibrating table and heavy liquid density-based separation.

Carbonate and dust contamination were removed by HNO_3 treatment of the samples. Mica separates from seven samples were selected for single-grain fusion dating. The samples were packed in aluminum foil packages and stacked in an aluminum tube that was irradiated for 18 hr in the CLICIT facility of the Oregon State University TRIGA Reactor. For both irradiations the neutron flux was monitored by standard bracketing with the DRA sanidine standard with an age of 25.52± 0.08Ma, modified from Wijbrans et al. (1995) to be consistent with Kuiper et al. (2008).

Single-grain fusion and step heating experiments were carried out in the Vrije University Amsterdam argon geochronology laboratory with 25 W CO_2 laser heating samples loaded on Cu-trays (185 individual 2-mm diameter, 3-mm-deep holes for single grains, and 6-mm-diameter holes for the incremental heating of fine sericite). The sample holder was connected to a three-stage extraction line and a quadrupole mass spectrometer (Schneider et al., 2009). Data were reduced in ArArCalc 2.50 (Koppers, 2002). Procedure blanks were monitored, and diluted air shots were measured in the sequence to track mass discrimination.

4. Results

4.1. Structural Mapping and Kinematics of Ductile Deformation

Field work has been conducted with the aim of inferring the kinematics and relative sequence of deformation phases that are associated with the burial and the exhumation of rocks exposed on the island of Skopelos. As such our fieldwork entailed a detailed mapping of ductile structures including foliation planes and related stretching lineations and shear sense indicators (Passchier & Trouw, 1996; Simpson & Schmid, 1983) as well as fold structures. Structural mapping was done on the basis of the geological map of Skopelos (Matarangas, 1992) and led to the revision of the map on some fault structures and their kinematics (Figure 2), a detailed discussion of which is beyond the scope of this contribution. The field data are summarized in map and cross-sectional view (Figures 2a and 2b and 3a–3c) as well as in stereographic projections (Figures 3d and 3e). Based on overprinting relations, the mapping of ductile fabrics yielded two distinct deformation phases, which are related to two different burial and exhumation cycles.

D_1 deformation phase consists of structures that have been observed in the Pelagonian and Glossa units as well as in the lowermost formation of the Palouki unit. However, D_1 structures are absent in the younger sedimentary cycle (Mesoautochtonous unit and in the upper formations of the Palouki unit). The remnants of a first generation of tight-isoclinal folds (F_1) and an associated axial planar cleavage (S_1) are preserved in many outcrops (Figures 4c and 4d) and some of our samples (Figures 5a, 5d, and 5e). S_1 foliation planes and L_1 stretching lineations are defined by white mica, chlorite, and calcite. Fold axes of F_1 tight-isoclinal, cylindrical folds are mainly trending NE-SW and have both NW and SE vergence (Figures 3c and 3e). In a few occasions F_1 sheath folds have been observed implying intense noncoaxial ductile shear (Figure 4a). In outcrops that exhibit S_1 foliation surfaces, L_1 stretching lineations were identified, showing approximately NW-SE trends (Figure 3a). Associated kinematic indicators show both top-to-the-NW and top-to-the-SE sense of shear in agreement with the double vergence (NW and SE) of F_1 tight-isoclinal folds. D_1 structural features are generally not bound to major shear zones but are within the Pelagonian, Glossa, and the lowermost formation of the Palouki units. However, the distribution is not homogenous; NW-SE stretching lineations and associated top-to-the-NW - and SE shear sense indicators are the most abundant in the Upper Paleozoic-Carnian metasediments of the Pelagonian unit (Figures 3a and 3b). No convincing overprinting relations between the top-NW and top-SE shearing have been observed, probably due to the strong post-D_1 overprint.

D_2 structures, which overprint D_1 structures (Figures 4a, 4b, 4d, and 4g and 5a, 5d, and 5e) are more abundant, are found in many outcrops and in all geological units of Skopelos. The D_2 phase was characterized by the formation of a pervasive foliation (S_2) defined by fine-grained white mica, chlorite, solution surfaces, and in case of marbles calcite (Figure 5). S_2 corresponds to the axial planar cleavage of tight-isoclinal F_2 folds that trend NW-SE and have both SW and NE vergence (Figures 3c and 3e, 4g, and 5a). In the Pelagonian and Glossa units, as well as in the lowermost formation of the Palouki unit, F_2 structures fold the S_1 tectonic foliation (Figures 4d and 4g and 5a and 5d), while in the Mesoautochtonous unit and in the upper

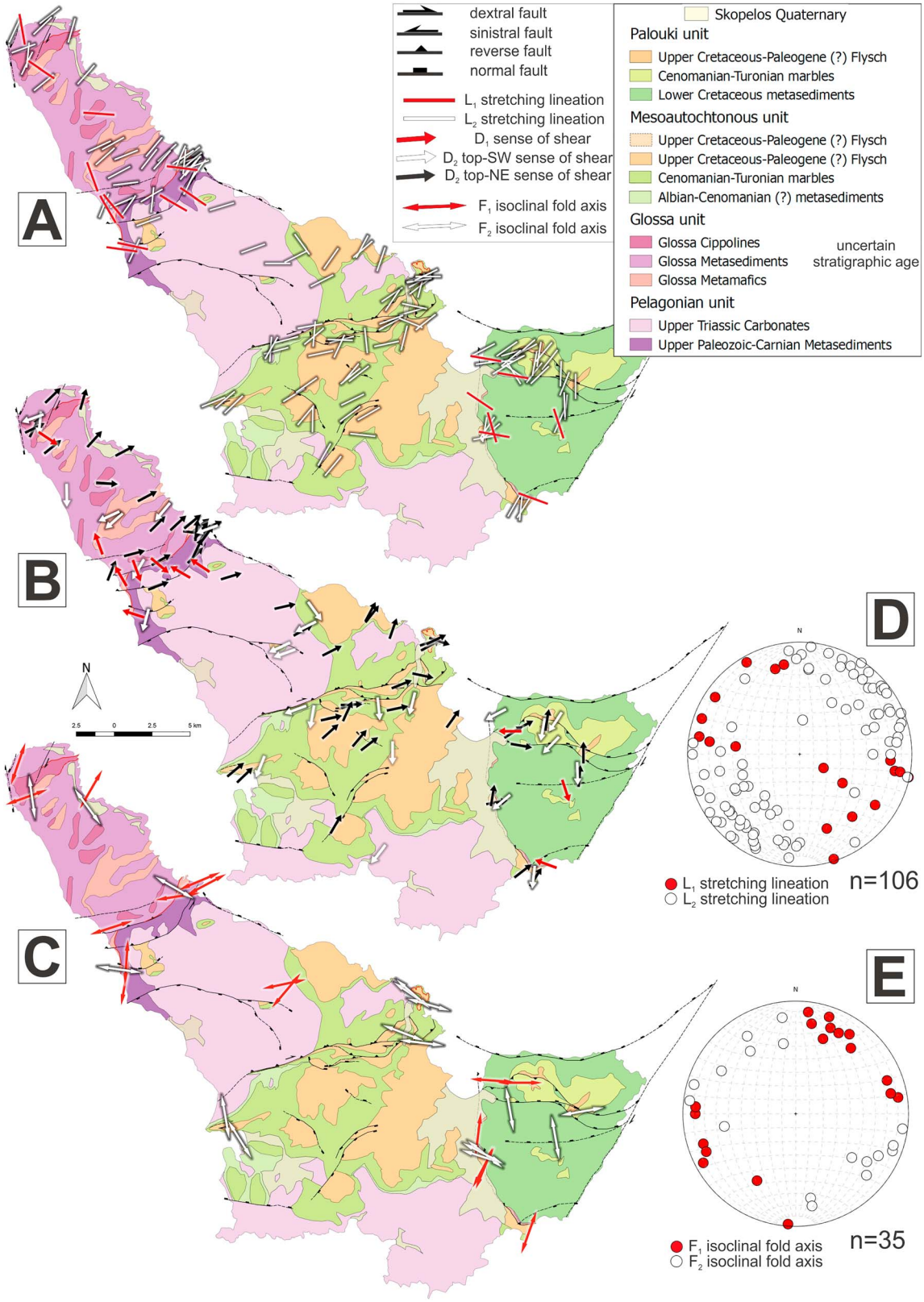

Figure 3. Plots of key structural measurements on Skopelos. (a) Map of stretching lineations. (b) Map of stretching lineations associated with kinematic indicators. (c) Map of isoclinal fold axes. (d) Stereographic projection of stretching lineations. (e) Stereographic projection of isoclinal fold axes.

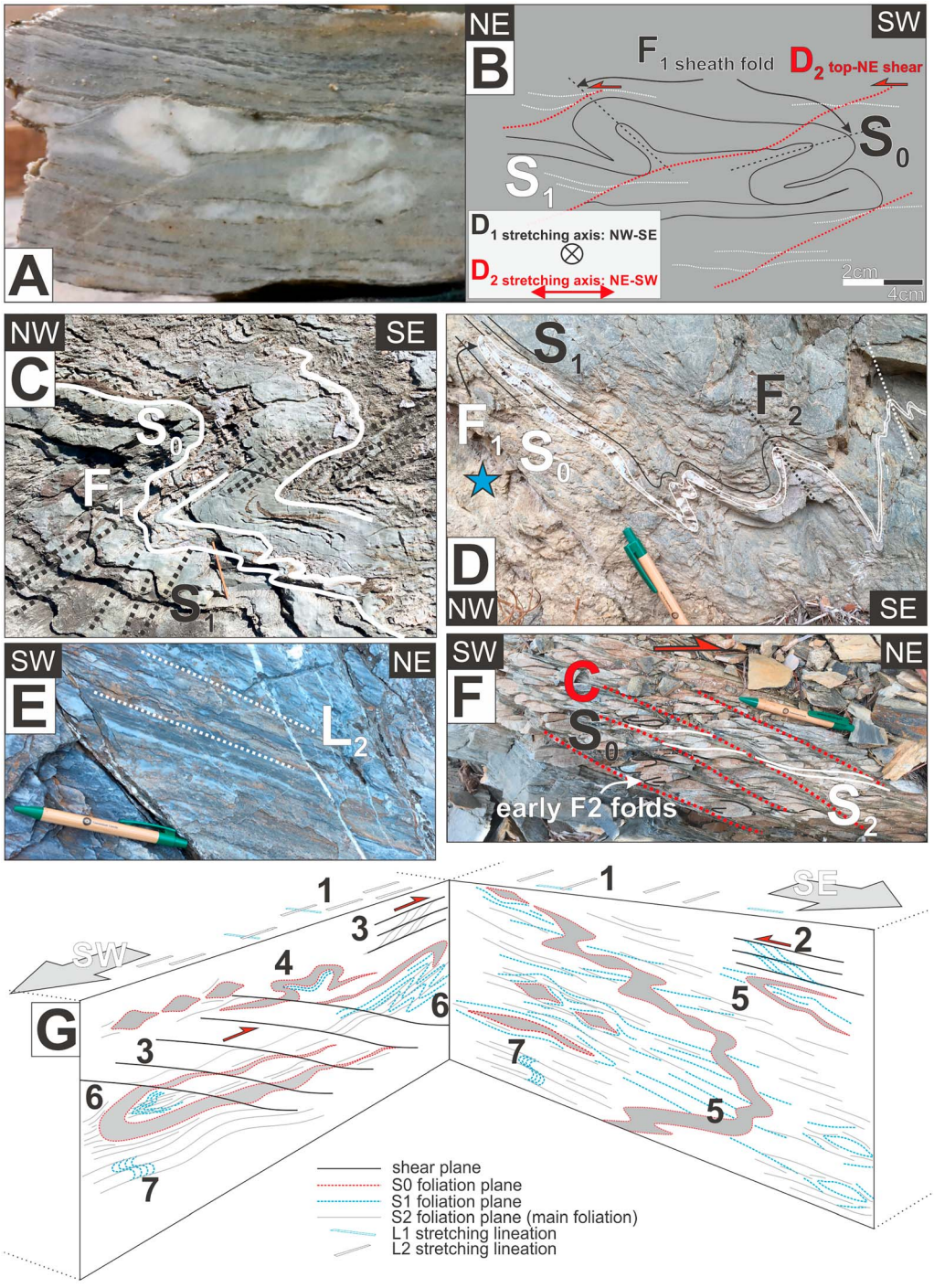

Figure 4. Structural interpretation of key observations. (a and b) Photo and related drawing of a NW-SE trending sheath fold overprinted by top-to-the-NE C-prime shear bands in the Glossa unit. The sections are parallel with the L_2 stretching lineation. (c) SE-verging F_1 isoclinal fold with well-preserved S_1 axial planar cleavage in the Pelagonian unit. The section is parallel with the L_1 stretching lineation. (d) Isoclinal F_1 fold refolded by close to tight F_2 folds at location 13.2 (for location see Figure 2a). The blue star represents the location of sample 13.2 used for $^{40}Ar/^{39}Ar$ single-grain fusion dating (Figure 8). The section is parallel with the L_1 stretching lineation. (e) NE-plunging L_2 stretching lineation in the marbles of the Glossa unit. (f) Top-to-the-NE C-S fabric in the Upper Cretaceous-Paleogene flysch of the Mesoautochtonous unit. Note that the early D_2 isoclinal folds are cut by the shear planes. The section is parallel with the L_2 stretching lineation. (g) Idealized NE-SW and NW-SE sections showing the typical structures observed in the Pelagonian, Glossa, and the basal formation of the Palouki units. 1: Scarce NW-SE plunging L_1 stretching lineations and dominant NE-SW plunging L_2 stretching lineations (Figure 3a and d). 2: top-to-the-NW shear criteria (Figure 3b). 3: top-to-the-NE shear criteria (Figure 3b). 4: section of noncylindrical F_1 fold (sheath fold; Figure 4a and b). 5: remnants of tight-isoclinal F_1 folds with either NW or SE vergence. In the hinge zones of these folds the S_1 foliation is well-preserved (Figure 4c), otherwise obliterated by the pervasive S_2 foliation. 6: F_2 folds folding both S_0 and S_1 foliations (Figure 4d). 7: S_1 foliation crenulated by the S_2 foliation (Figure 5a).

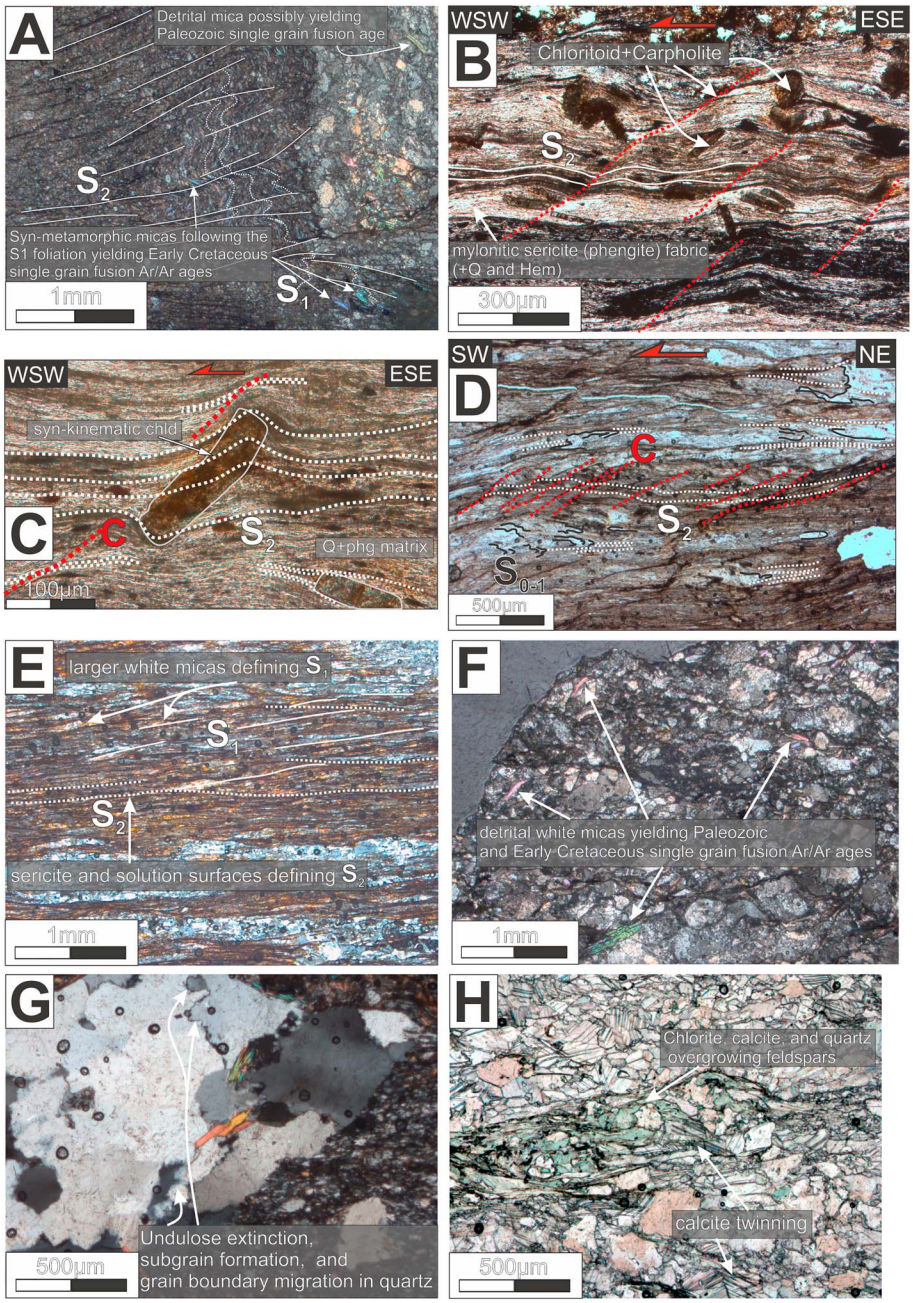

Figure 5. Interpretation of microscope images. Images from a to g were captured with cross-polarized light; image h was captured with plain-polarized light. For sample locations see Figure 2a. (a) Photo of sample 8.1 highlighting the two tectonic foliations (S_1 and S_2) present in the Pelagonian unit and the larger (≥200μm) white mica crystals which were picked for $^{40}Ar/^{39}Ar$ single-grain fusion dating (Figure 8). Note that the majority of the micas define the S_1 foliation and thus associated to D_1 deformation, but some grains of detrital origin also occur. The section is parallel with the L_2 stretching lineation. (b) Photo of sample 3.3 showing the mylonitic S_2 foliation developed during top-to-the-WSW shearing. Chloritoid porphyroblasts contain remnants of carpholite and are swimming in a matrix of phengite, quartz, and hematite. This sample was used for P-T calculations (Figure 7) and for $^{40}Ar/^{39}Ar$ fabric dating (sample 3.3 on Figure 9). The section is parallel with the L_2 stretching lineation. (c) Photo of sample 3.3 showing a synkinematic chloritoid porphyroblast with respect to top-to-the-WSW shearing. The section is parallel with the L_2 stretching lineation. (d) Photo of sample 7.2 from the Glossa unit showing the remnants of the disrupted $S_{0\text{-}1}$ foliation folded into tight-isoclinal folds, and the main S_2 foliation defined by very fine-grained sericite (for $^{40}Ar/^{39}Ar$ fabric age of this sample see Figure 9) and dissolution surfaces. Top-to-the-SW C′-type shear bands developed during and/or after the formation of the S_2 foliation. The section is parallel with the L_2 stretching lineation. (e) Photo of sample 7.1 from the Pelagonian unit showing S_1 foliation defined by larger white micas (≥200μm) and S_2 foliation defined by fine grained sericite and solution surfaces (for $^{40}Ar/^{39}Ar$ fabric age of this sample see Figure 9) The section is parallel with the L_2 stretching lineation. (f) Photo of sample 7.2 from the Mesoautochtonous flysch unit showing detrital white mica crystals which were used for $^{40}Ar/^{39}Ar$ single-grain fusion dating. (g) Photo of sample 1.2b from the Glossa unit showing the dynamic recrystallization of quartz. (h) Photo of sample 19.1 from the metabasalts of the Glossa unit showing extensive growth of chlorite and calcite at the expense of the original basaltic mineral assemblage.

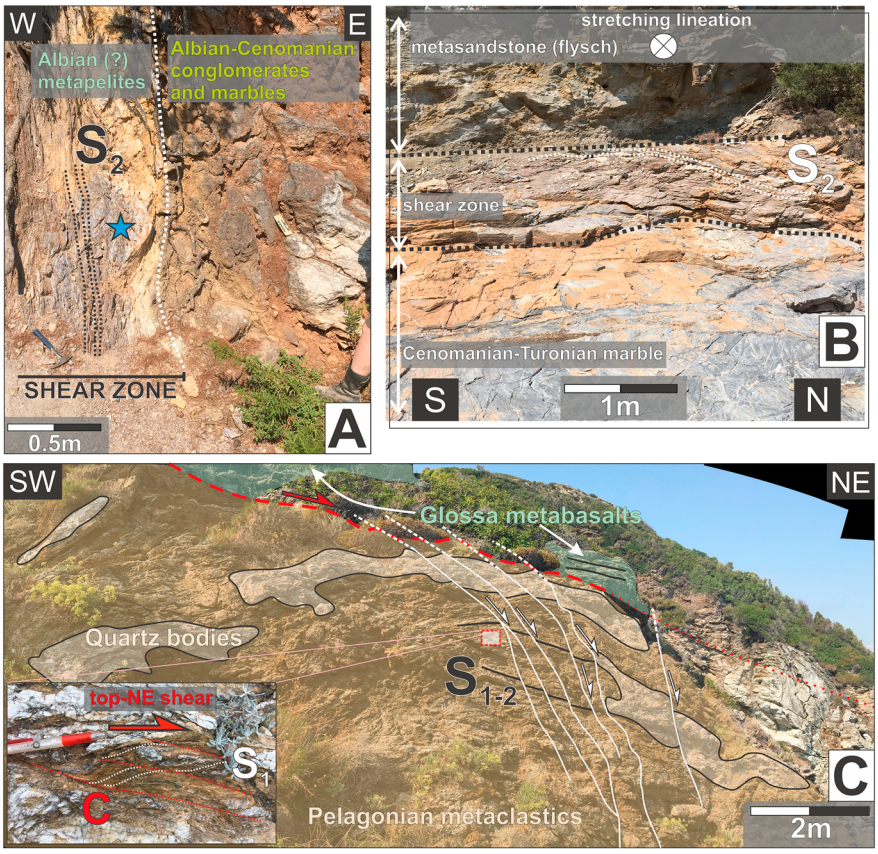

Figure 6. Interpretation of key outcrops. For outcrop locations see Figure 2a. (a) Shear zone at location 3.3 in Al-rich metapelites separating the Pelagonian and Mesoautochtonous units. Blue star represents the location of the sample used for P-T calculations (Figure 7) and $^{40}Ar/^{39}Ar$ S_2 fabric dating (Figure 9). (b) Top-E shear zone localized at the stratigraphic contact between the Cenomanian-Turonian marbles and Upper Cretaceous-Paleogene Flysch of the Mesoautochtonous unit at outcrop 16.2.Note that the shear zone is subparallel with the mylonitic S_2 foliation. (c) Contact between the Pelagonian and the Glossa units at location 23.1. The contact is characterized by well-developed metamorphic foliation, intense and clear NE-SW trending stretching lineation, top-NE ductile shear, thick bodies of secondary quartz, and late-stage normal faults which cut through the sheared contact.

formations of the Palouki unit F_2 structures fold the S_0 bedding. Rare occurrences of NE-SW trending F_2 noncylindrical sheath folds are confined to zones of localized ductile strain. S_2 foliation planes exhibit strong stretching lineations observed on calcite (Figure 4e), white mica, and chlorite, trending NE-SW (measured in more than 80 outcrops; Figures 3a and 3d). Associated kinematic indicators show the dominance of top-to-the-NE shear sense (Figures 3b and 4f), but a significant number of top-to-the-SW shear sense indicators have also been found (Figures 3b and 5b and 5d). D_2 structures also show largely distributed pattern; however, several tectonic contacts have been found with localized ductile deformation related to top-to-the-NE or top-to-the-SW tectonic transport (Figure 6). The S_2 main foliation and F_2 isoclinal folds are in most cases bent or cut by top-to-the-NE shear bands (Figure 4f) or shear zones that are observed to be gradually replaced by semibrittle to brittle normal faults (Figure 6c). These observations suggest that the early D_2 phase is characterized by isoclinal folding (F_2) and the formation of the main foliation (S_2) and top-to-the-SW shearing (Figures 5b and 5c), which is followed by top-to-the-NE shearing (late D_2; Figures 4f and 4g). Top-to-the-NE shearing is the last phase of ductile deformation we have observed on the island. The description and discussion of the newly established fault pattern (Figure 2a) are out of the scope of present contribution.

4.2. D_2 Shear Zones

Figure 6c shows the only clear outcrop (outcrop 23.1, for location see Figure 2a) exhibiting the contact between the Pelagonian and the Glossa units. There, pervasive NE-SW trending stretching lineations with

top-NE sense of shear as indicated by C-S structures (Figure 6c) are observed, as well as thick veins and bodies of secondary quartz and intense folding. The deformation is largely accommodated in the Pelagonian metaclastic rocks below the contact delineating a 8- to 15-m-thick zone of localized ductile deformation. The ductile fabric of the shear zone is cut by a series of semibrittle to brittle normal faults dipping to the North showing a gradual change in the style of extensional deformation from ductile shearing to normal faulting (Figures 6c).

Note that the top-NE shear zone has been tilted toward the NW due to a series of brittle, oblique strike-slip/reverse faults during a younger stage of deformation resulting in a NE-SW orientation of the shear zone in map view (Figures 2a and 2c).

We also found that D_2 deformation often localized within narrow (1- to 10-m-thick) shear zones, which are either parallel to the stratigraphic layering (Figure 6b or see Figures 2a and 2c for map view) or reactivated already existing tectonic contacts (Figure 6c). The sense of shear within these shear zones is top-NE or top-E. A D_2 tectonic contact has also been found at the base of Mesoautochtonous unit separating the Pelagonian unit from the Cenomanian-Turonian basal conglomerates and marbles (Figure 6a). The shear zone consists of very fine grained, foliated, high-Al metapelites. The metapelites exhibit intense ductile deformation; they have a very closely spaced foliation and a top-WSW C′-type shear bands (Figure 5b). In contrast, the conglomerates and marbles show no enhanced stretching or layer-perpendicular shortening. The subvertical orientation of the foliation and the shear zone is due to late-stage fault-related folding caused by a transpressive fault running at a distance of roughly 100m from the outcrop (Figure 2a). Back-rotation of the shear fabric into its prefolding position yielded a ENE-WSW stretching direction for the shear zone with associated shear fabric implying top-WSW sense of shear, which means WSW-ward movement of the conglomerate-marble sequence with respect to the metapelites and the Pelagonian unit. The significance of this contact was proven by microstructural and petrological analysis of the sample from this outcrop (sample 3.3), which is described in the next section (3.3).

4.3. Metamorphic Conditions

More than 50 thin sections were analyzed in an effort to characterize as precisely as possible microscale deformation processes and metamorphic mineral assemblages associated with the different formations and deformation phases. All outcrops of the main units on Skopelos display evidence of synmetamorphic, microscale processes such as dissolution creep, white mica (re)crystallization (Figures 5b and 5c), calcite twinning (Figure 5h), quartz subgrain formation and grain boundary migration (Figure 5g), and chlorite-calcite growth (Figure 5h). Chlorite growth is especially characteristic of the metabasaltic formation of the Glossa unit (Figure 5h) and is commonly accompanied by albite and epidote growth. Investigation of metamorphic mineral assemblages did not reveal significant differences in metamorphic grade between the different tectonic units of Skopelos, or between D_1 and D_2 deformation phases. Foliation S_1 is defined by larger white mica grains ($\geq$250μm; Figures 6a and 6c) as compared with S_2, which is commonly defined by mylonitic sericite fabric which overgrowing the preexisting larger micas of the S_1 foliation (Figures 6b and 6c). The observed mineral assemblages and microscale deformation processes are consistent with metamorphism under greenschist-facies conditions for both D_1 and D_2 events.

An exception to the general greenschist facies conditions of D_1 and D_2 ductile fabrics was found in outcrop 3.3 (Figure 6a); the sample collected from the mylonitic metapelites exhibits an entirely different mineral content and associated PT conditions associated to D_2 deformation as described in detail below. Representative mineral analyses from this outcrop are reported in the Table A1, whereas the whole-rock composition is listed in Table A2. In sample 3.3 (Figure 6b), chloritoid porphyroblasts (6vol%) are set in a very fine-grained mylonitic fabric defined by phengite (51%) + quartz (38%) + hematite (4%). Most of the chloritoid crystals are synkinematic (Figure 5c) with respect to the shearing event (top-to-the-WSW) that produced the mylonitic foliation and often contain S-shaped quartz inclusion trails, although larger, pretectonic crystals have also been observed. Chloritoid crystals have grown at the expense of and contain inclusions of carpholite, indicating progressive crystallization typically under high-pressure/low-temperature conditions (Goffé et al., 1973; Pourteau et al., 2014; Vidal et al., 1992, 1994), a rather common feature of blueschist-facies metapelites from various Tethyan localities (Agard et al., 2001; Goffé et al., 1988; Oberhänsli et al., 1998; Plunder et al., 2013; Trotet et al., 2006; Vidal & Theye, 1996).

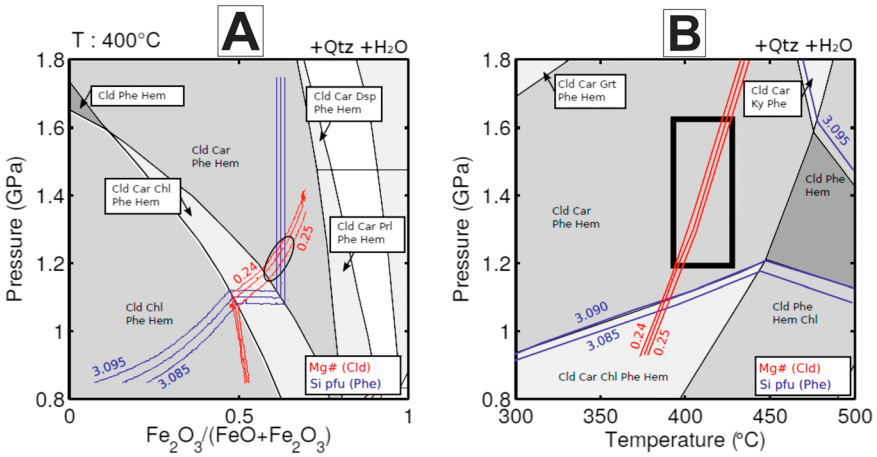

Figure 7. PX and PT sections for sample 3.3 (for sample location see Figure 2a, for thin section and outcrop images see Figures 5b and 5c and 6a). Quartz (SiO_2) and water (H_2O) were assumed in excess. (a) PX section calculated for T=400°C. (b) Isochemical PT section.

There is a continuum in chloritoid crystallization from the larger relictic grains to the smaller synfolial ones as attested to by their overlapping Mg# values with the rims of the synfolial grains displaying the highest values (see Table A1), interpreted to have recorded the highest metamorphic grade (see Pourteau et al., 2014, their Figures 7b–7d). To a first approximation, and according to the calculations of Pourteau et al. (2014) in the FMASH system, the range of observed chloritoid Mg# values (~0.19 to ~0.25) in the divariant chloritoid-carpholite field is consistent with temperatures between 350 and 450°C in the pressure range 1-2GPa.

Pressure and temperature conditions that prevailed during shearing of sample 3.3 were assessed using Gibbs free-energy minimization (Connolly, 2005; Connolly, 2009) and mineral and bulk-rock data from Tables A1 and A2. The solution models used are Ctd (HP) for chloritoid, mica (CHA1) for white mica, Gt (GCT) for garnet, Chl (HP) for chlorite, and Carp for carpholite (http://www.perplex.ethz.ch/).

The presence of hematite in the sample does not allow for a simple calculation of phase equilibria assuming all Fe as Fe2+. Even if measured Fe3+ values were available, we still cannot know how Fe2+/Fe3+ could have possibly changed with time during metamorphism. To circumvent this problem, we introduced Fe3+ as an unknown variable. This, of course, increases the dimensionality of the problem (i.e., from two to three independent variables) and makes calculations more complicated. Our approach was to compute several 2D P-X sections assuming constant temperature (350, 375, 400, 425, and 450°C), where X is the bulk-rock Fe2O3/(Fe2O3+FeO) ratio (in wt.%) that becomes zero (0) when all Fe is present as Fe2+ and one (1) when all Fe is present as Fe3+. The presence of hematite and Fe2+-bearing minerals in 3.3 suggests that X lies between 0 and 1.

We simplified the pelitic composition by ignoring the minute amounts of Na, Ca, and Ti and assumed that the system is saturated in H_2O (water) and SiO_2 (quartz; i.e., K2O-FeO-Fe2O3-MgO-Al2O3-SiO2-H2O system). The calculated misfit between modeled and measured mineral compositions (see Hunziker et al., 2017, their Equation 1) is minimized for temperatures between 400 and 425°C. For an X value of ~0.62, the crossing of the Si-in-Phe (atoms per formula unit or apfu; see Table A1) and Mg#-in-Cld isopleths at these temperatures occurs at P~1.2 and 1.6GPa, respectively. Figure 7a is a P-X section for T=400°C. The corresponding *P-T* section for that particular composition is depicted in Figure 7b. Considering the uncertainties due to ferric iron, the compositional isopleths of Mg#-in-chloritoid, Si-in-phengite, and the thermodynamic stability of the assemblage (Car-Cld-Qz-Phe-Hem; mineral abbreviations after Whitney & Evans, 2010) suggest that metamorphic recrystallization should have taken place at T=400–425 ± 25°C and 1.2–1.6 ± 0.2GPa. This is in agreement with but refines much more rigorously the *P-T* bracket inferred earlier, based on thermodynamic modeling of carpholite-chloritoid equilibria alone (Pourteau et al., 2014). Our figures represent a robust estimate of the *P-T* conditions under which the observed mylonitic foliation

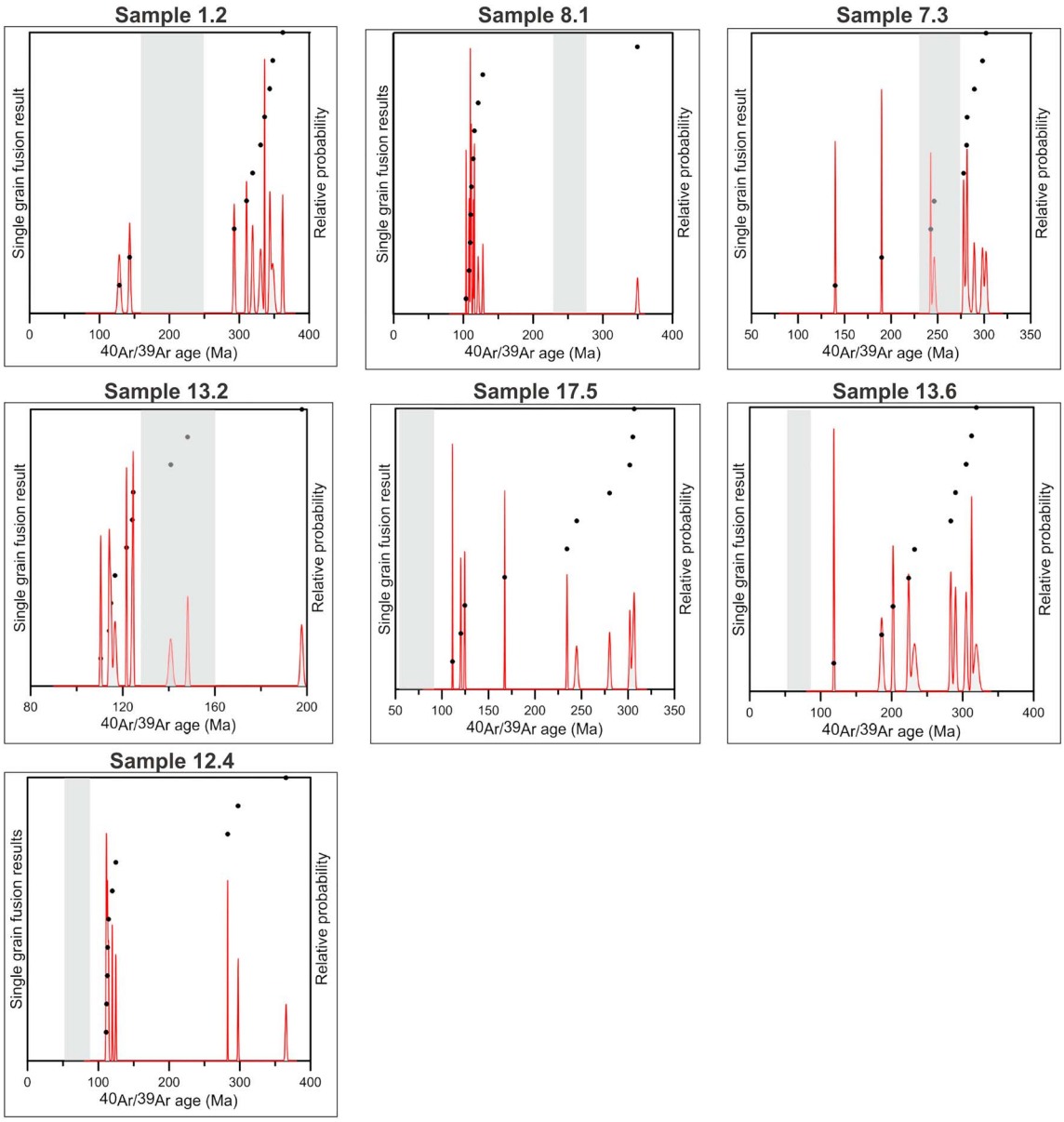

Figure 8. Diagrams of $^{40}Ar/^{39}Ar$ single-grain fusion dating experiments on larger (≥200μm) white mica crystals. The diagrams show the age distribution of single mica crystals (black dots) and the relative probability of the results (red line). The relative probability is a function of the absolute age and the corresponding σ1 error of a single mica grain. If individual error is small with respect to the bin size one gets a spikier representation of the peaks. Grey stripes indicate the stratigraphic extent of the units of which the samples are derived from. For sample locations see Figure 2a. For thin section images of samples 8.1 and 12.4 see Figures 6a and 6d, respectively.

formed in sample 3.3. The calculated thermodynamic pressure here is essentially equal to the mean stress but could deviate from lithostatic (Moulas et al., 2013, 2018).

4.4. $^{40}Ar/^{39}Ar$ Dating

4.4.1. Single-Grain Fusion Experiments

The results of single-grain fusion experiments are presented on Figure 8. The plots show largely heterogeneous distributions of ages, which could theoretically indicate either that (1) the timing of closure was heterogeneous (meaning multiple geological events), (2) inherited argon is unequally removed from the crystals, or (3) there is variable amount of excess argon. In our case two main age groups can be

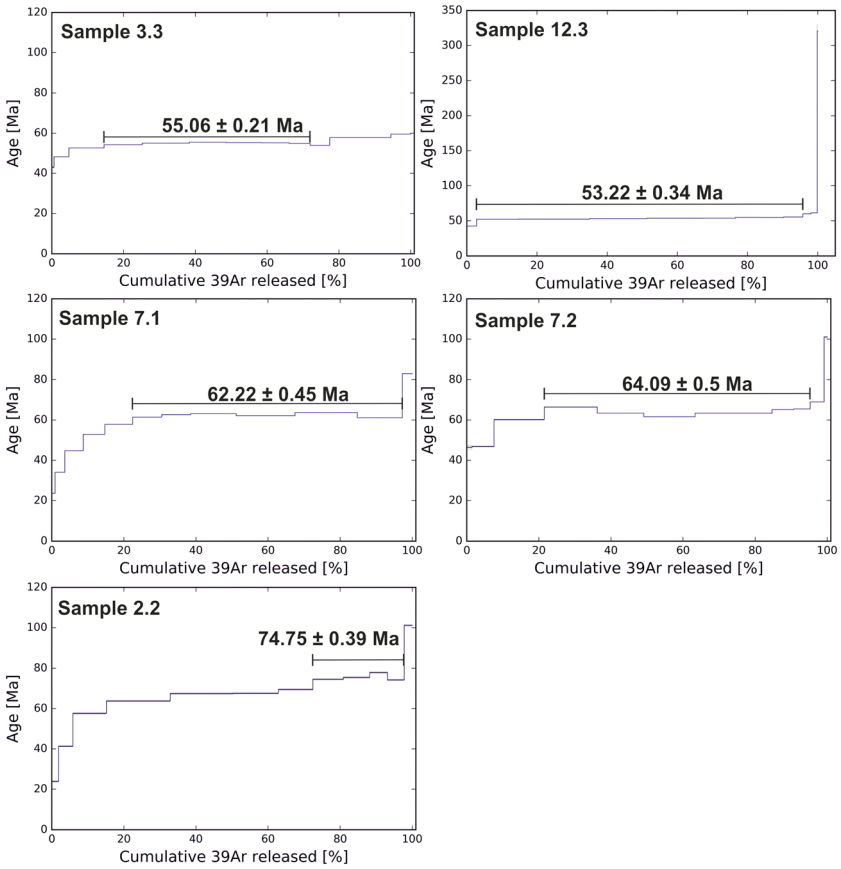

Figure 9. Diagrams of $^{40}Ar/^{39}Ar$ step heating fabric dating experiments on fine grained white micas (sericite). The horizontal axes show the cumulative ^{39}Ar released during the step heating, while vertical axes show the age of Ar-loss. For sample locations see Figure 2a. For thin section images of samples 3.3, 7.2, and 7.1 see Figures 5b–5e, respectively. Note that the $\sigma 1$ error [Ma] of each heating step is plotted with blue lines which tend to be very close to the result function (black line).

distinguished based on the $^{40}Ar/^{39}Ar$ dating: a Paleozoic (>250Ma) group, and an Early Cretaceous, ~105-135Ma group. Especially samples 8.1 and 12.4 show clear peaks of Early Cretaceous ages showing that most of the white micas in these samples date an event in the Early Cretaceous. The presence of Paleozoic single-grain fusion ages in the pre-Early Cretaceous metasedimentary formations (Pelagonian, Glossa, and the basal formation of the Palouki units) implies that temperature reached during the Early Cretaceous event was not high enough (<500°C) to reset the Ar-system of all the white micas by thermally activated volume diffusion, allowing in some grains the Variscan protolith ages to be preserved. Early Cretaceous ages thus most likely represent deformation-driven recrystallization and cannot be interpreted as cooling ages (Warren et al., 2012).

This means that the Early Cretaceous grains provide direct constraints for the timing of a tectono-metamorphic event in the pre-Early Cretaceous formations. On the other hand, Paleozoic ages are likely to represent the cooling of the Variscan basement rocks or alternatively Variscan deformation events. The fact that the signal of detrital, Variscan grains, and newly formed Early Cretaceous grains can be separated shows the strength of the single-grain fusion approach as long as the temperature of metamorphism does not exceed 500 °C (for more details about the single-grain fusion approach see Uunk et al., 2018). For example, in case of sample 8.1, which comes from the metaclastic series of the Pelagonian unit, the majority of the white micas define the S_1 foliation of the rock which formed during a metamorphic event (Figure 5a). However, the sample also contains larger clasts with detrital white micas (Figure 5a). Looking at the age distribution of sample 8.1 in Figure 8, the result shows a very good agreement with the observations in the thin section: a clear Early Cretaceous peak (nine grains with similar ages) defining the metamorphic event, but also one

detrital grain which shows Variscan origin and proves that resetting in the Early Cretaceous was not achieved by thermal diffusion, but by deformation-induced crystallization.

Grains with ages between the Early Cretaceous and the Paleozoic—that are difficult to explain from a geological point of view—might be the consequence of unequally removed inherited argon leading to mixed ages intermediate between the two recorded events (Figure 8).

4.4.2. Step Heating Experiments: Dating S_2 Fabrics

The results of step heating experiments on the S_2 sericite foliations are presented on Figure 9. Age spectra show a dominance of 53-75 Ma, documenting the S_2 fabric-forming event in the rocks of Skopelos. The samples from the Mesoautochtonous unit (samples 3.3 and 12.3) show younger ages than the samples from the Glossa and Pelagonian units (samples 7.1, 7.2, and 2.2). This might be due to earlier fabric formation in those samples, or alternatively to the presence of minor amount of Early Cretaceous mica fragments in the ground mass of samples 7.1, 7.2, and 2.2. The determination of the ages based on the spectra seems robust in all samples except for sample 2.2 where the more complicated age spectra would also allow to define a younger age of ca. 65Ma. However, based on the number of steps (4 versus 3) we prefer to accept the ~75Ma age for sample 2.2 (Figure 9). Staircase-shaped age spectra of samples 7.1 and 2.2 imply that a younger (probably ~25Ma) thermal overprinting event affected these samples. Since this event is not present in all samples, the regional significance of this overprint is not clear.

5. Interpretation of Results

5.1. Late Jurassic-Early Cretaceous Evolution of Skopelos

D_1 deformation phase on Skopelos is defined by the remnants of a first foliation (S_1 on Figures 5a, 5d, and 5e), NW-SE trending stretching lineations, and related shear sense indicators showing top-NW and top-SE sense of shear (Figure 3a and 3b). A distinct group of first-generation, cylindrical isoclinal folds (F_1) have NE-SW trending fold axes (Figure 3c), which fits to the NW-SE shearing suggested by the L_1 stretching lineations and associated shear sense indicators. D_1 structures are limited to the Pelagonian, Glossa, and the oldest formation of the Palouki units.

Single-grain fusion $^{40}Ar/^{39}Ar$ dating of white micas allows us to define a clear fabric-forming event in the Early Cretaceous (~105-135 Ma; Figure 8) that by multigrain dating would have been partly obscured by admixing of a Variscan component in the sample material. In case of the Pelagonian, Glossa, and in the oldest formation of the Palouki units, the single-grain fusion approach allows for separating detrital, Variscan micas from grains defining the S_1 foliation (Figure 5a). Since the temperature during D_1 deformation was not high enough to reset the detrital grains by thermal diffusion, we conclude that the Early Cretaceous ages are achieved by deformation-induced crystallization and treat them as direct time constraints for the formation of the S_1 foliation and thus the timing of D_1 deformation phase. The lack of any remnants of a higher-temperature mineral association and the presence of nonreset detrital white micas in the relevant formations suggest that metamorphic conditions during D_1 phase did not exceed greenschist facies.

The Pelagonian unit of Skopelos was deposited on the passive margin of the Pelagonian continental basement facing the Neotethys/Vardar ocean (Figure 11a). In our interpretation, the Glossa unit represents the deep water-facies equivalent of the Pelagonian unit and was deposited coevally on the distal Pelagonian margin and/or on the ocean-continent transition zone (Figure 11a). A similar reconstruction has already been proposed linking the Eohellenic nappe (Jacobshagen et al., 1978) and as part of that the Glossa unit (Matarangas, 1992) with the Vardar ocean.

The origin of the Palouki unit, the stratigraphic range of the basal formation of the unit, and the contact between the basal and the upper formations have not been clarified so far (Matarangas, 1992). Our $^{40}Ar/^{39}Ar$ white mica single-grain fusion ages from the basal formation of the Palouki unit show a roughly 110-125 Ma white mica population in the formation. The fossils found in the basal Palouki formation provide a Late Jurassic-Early Cretaceous possible range of deposition (Matarangas, 1992). Our $^{40}Ar/^{39}Ar$ ages imply that the formation was buried and metamorphosed around 110-125 Ma (sample 13.2 in Figure 8), which brackets the possible depositional range of the basal Palouki formation between ~130 and 160 Ma. In our view the basal formation of the Palouki unit was most likely deposited on top of the Eohellenic units (in

the sense of Jacobshagen et al., 1978), prior to Early Cretaceous metamorphism of the Pelagonian margin (Lips et al., 1998; Most, 2003; Schermer et al., 1990; Walcott, 1998), in front of the advancing ophiolitic thrust sheet(s). This idea is supported by deep water facies characteristics of the sedimentary succession (Matarangas, 1992) and blocks of serpentinites and mafic volcanics in the formation. In this sense the basal Palouki formation is similar to the subophiolitic mélange mapped on Evia (e.g., Danelian & Robertson, 2001), in the northern part of the Pelagonian zone (e.g., Sharp & Robertson, 2006), or in the Internal Dinarides (e.g., Gawlick et al., 2009; Schmid et al., 2008).

Following the deposition of the lowermost Palouki formation, the Pelagonian margin was overthrust by the Neotethyan ophiolites and consequently buried to greenschist facies conditions. The Glossa unit on Skopelos was most likely emplaced on top of the Pelagonian unit during the Early Cretaceous D_1 phase. This scenario is compatible with the idea of passive margin inversion during obduction (Figure 11b) and is also supported by commonly found SE and NW verging, isoclinal F_1 folds as well as NW-SE trending L_1 stretching lineations in the proximity of the contact, implying a NW-SE trend of movement (Figure 3).

As it is suggested by our single-grain fusion $^{40}Ar/^{39}Ar$ ages (Figure 8), S_1 fabric formation in the Pelagonian, Glossa, and the lowermost formation of the Palouki units ceased ~110-105 Ma suggesting the exhumation of these units above the brittle-ductile transition zone. The formations were subsequently transgressed by the Mesoautochtonous unit and the upper formations of the Palouki unit from the latest Albian-Early Cenomanian (~100-95 Ma; Matarangas, 1992), implying surface exposure of the older units. The $^{40}Ar/^{39}Ar$ ages and the stratigraphical constraints together constrain the timing of D_1 exhumation for the late Early Cretaceous.

5.2. Late Cretaceous-Paleogene Evolution of Skopelos

$^{40}Ar/^{39}Ar$ sericite S_2 fabric ages of present study (Figure 9) define a latest Cretaceous-earliest Eocene period of ductile fabric formation (S_2 main foliation) in all units of Skopelos. This foliation is pervasive on the whole island, and its formation is associated with NE-SW tectonic transport evidenced by stretching lineations and kinematic indicators (Figure 3b). Dating of fabrics related to D_2 deformation allows us to assign D_2 structures with a latest Cretaceous-earliest Eocene period. Without having a clear distinction between early and late D_2 deformations (top-SW versus top-NE shearing) in terms of metamorphic grade and mineral associations, it is difficult to assign the S_2 fabric forming to either top-SW or top-NE shearing. The mylonitic fabric of sample 3.3. (Figures 5b and 5c) however shows a clear top-WSW sense of shear and a well-developed S_2 foliation that is dated to be ~55 Myr old. This and the observations that top-NE shearing usually affects an already existing S_2 foliation suggest that the D_2 fabric-forming event was predominantly associated with the top-SW shearing.

The metamorphic grade of D_2 phase is constrained by microscale deformation mechanisms and metamorphic mineral assemblages, which imply greenschist facies conditions for the rocks of Skopelos except for one blueschist facies shear zone (Figures 6a and 7) between the Pelagonian and Mesoautochtonous units. Considering the generally low metamorphic grade of the formations, we suggest that the rocks of Skopelos were not subducted to great depth together with the Pelagonian basement (e.g., Brun et al., 2016) during D_2 burial, but they were rather incorporated into an accretionary wedge between Pelagonia and Eurasia.

The top-SW distributed shearing (Figure 3b), thrusting of the Palouki unit on top of the Mesoautochtonous unit, and the top-WSW shear zone between the Pelagonian and Measoautochtonous units (Figure 11d) are correlated with the tectonic burial (thrusting) within the accretionary wedge during the latest Cretaceous-earliest Eocene.

The top-WSW blueschist facies shear zone at the base of the Mesoautochtonous unit consists of mylonitic metapelites that carries a foliation with a 55 Ma $^{40}Ar/^{39}Ar$ S_2 fabric age (Figures 5a, 7, and 8). The same high-pressure metapelites at the base of the Mesoautochtonous unit were described by Mposkos and Liati (1991) at the southwestern shore of the island, implying that the high-pressure shear zone is not only locally present between the Pelagonian and the Mesoautochtonous units. Since the high-pressure shear zone separates the Pelagonian and the Mesoautochtonous units, which are observed to have an erosional contact in most outcrops (Matarangas, 1992), we propose that parts of the erosional unconformity were activated during top-SW tectonic burial phase as a shear zone (Figure 11d). This view contradicts the previous

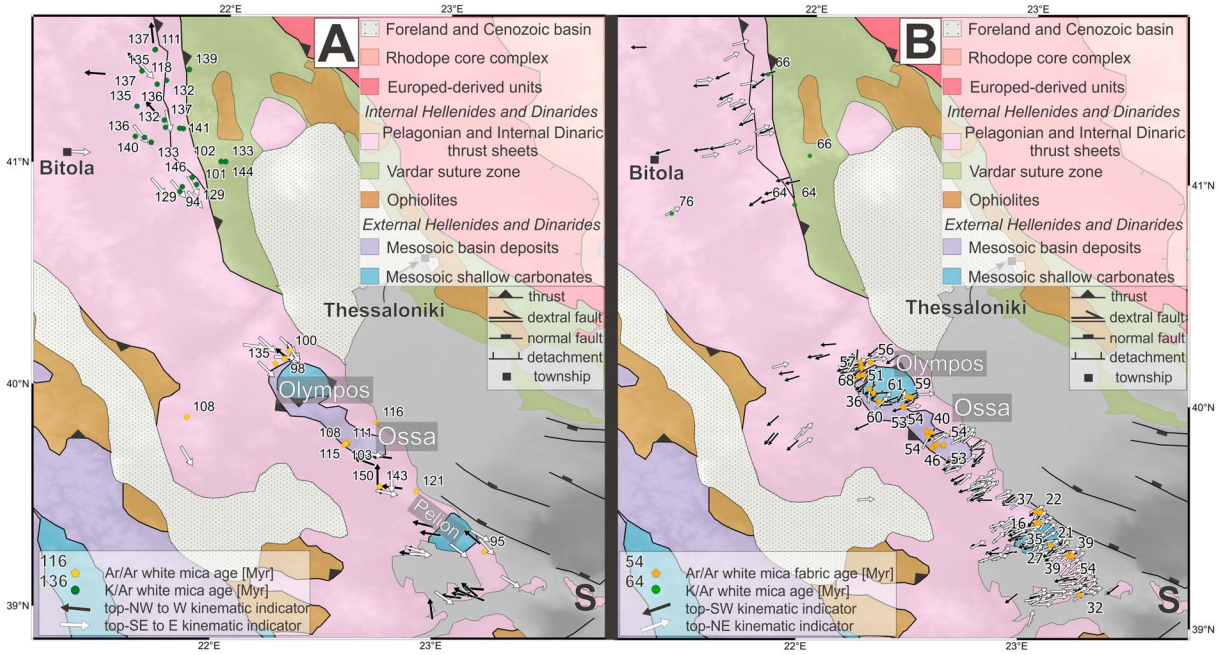

Figure 10. (a) Correlation of deformation phases in the Pelagonian zone. The basis for correlation are geochronological and kinematic data sets compiled from published data (Gerogiannis & Xypolias, 2017; Kilias et al., 2010; Lips et al., 1998, 1999; Most, 2003; Schermer et al., 1990; Walcott, 1998), which are comparable to our results from Skopelos. S=Skopelos. a, Correlation of D_1 phase: Early Cretaceous resetting of Ar-Ar and K-Ar systems coupled to observed top-NW or top-SE directed tectonic transport indicated by stretching lineations and associated kinematic indicators. Note that Early Cretaceous tectono-metamorphic events have also been reported from the Europe-derived units (e.g., Kydonakis et al., 2016); however, we focus exclusively on the Pelagonian zone. (b) Correlation of D_2 phase: latest Cretaceous-Paleogene Ar/Ar white mica fabric ages and K/Ar ages coupled to observed top-SW and top-NE tectonic transport.

interpretation, which reckoned with an erosional contact between the Mesoautochtonous and the Pelagonian units on the whole island (Matarangas, 1992).

The contact between the Pelagonian and the Glossa units has been described as a thrust based on the observation that the Glossa unit is structurally lying on top of the Pelagonian (Matarangas, 1992). According to our observations, the latest movement along this contact was top-NE shearing with normal kinematics (Figure 6c). However, we suggest that the Glossa unit was emplaced on top of the Pelagonian by a D_1 thrust or a reverse-sense shear zone preceding the activity of the D_2 top-NE normal-sense shear zone (Figure 11b). The D_2 shear zone thus reactivated or alternatively cut the Early Cretaceous (D_1) nappe contact between the two units (Figures 11d and 11e).

The dominant top-NE shearing (Figure 3b) overprints older D_1 or early-D_2 ductile structures (Figures 4b, 4f, and 4g) and occurred under decreasing temperatures as documented by the gradual change of ductile shearing to normal faulting (Figure 6c), within the same kinematic frame. We thus correlate the top-NE shearing on Skopelos with the extensional exhumation of the accretionary wedge above the brittle-ductile transition zone. According to our observations, this first stage of exhumation was largely accommodated by distributed top-NE shearing (Figure 3b), and by the formation of a few top-NE shear zones, which localized along pre-existing rheological contrasts, and dip subparallel to the main foliation (S_2; Figures 2, 6b and 6c, and 11e and 11f). These shear zones may have a minor to medium (few 100 or 1,000 m) of displacement (Figure 11f) and consequently do not cut out major parts of the stratigraphy. We suggest that the distributed and localized top-NE shearing together played an important role in the exhumation of Skopelos.

6. Implications for the Early Cretaceous Tectonics of the Pelagonian Margin

6.1. Correlation of Early Cretaceous Tectonic Events in the Pelagonian Zone

Early Cretaceous tectono-metamorphic events (D_1 in present work) have been reported from many locations along the Pelagonian zone (Figure 10a) and from its continuation into the Dinarides (Internal Dinaric thrust

sheets such as the Drina-Ivanjica and the Jadar-Kopaonik (Schmid et al., 2008). Single-grain $^{40}Ar/^{39}Ar$ laserprobe dating combined with petrological investigations showed the existence of a distinct blueschist to greenschist facies tectonic event in the region of the Pelion peninsula and the Ossa tectonic window (Lips et al., 1998, 1999; Figure 10a), while Rb/Sr and multigrain $^{40}Ar/^{39}Ar$ dating provided younger mixed ages (85-135 Ma) in the blueschist to greenschist facies rocks of the Olympos tectonic window (Schermer et al., 1990). Early Cretaceous metamorphism in the northeastern part of the Pelagonian zone was identified by K/Ar dating (Most, 2003; Figure 10a). Furthermore, remnants of high-temperature metamorphism during the Early Cretaceous are evidenced by dated anatectic melts (117±8 Ma) north from the Olympos window (Schenker et al., 2014). Walcott (1998) determined a large population of greenschist to amphibolite facies, NW-SE and weak E-W trending stretching lineations from the Thessaly-Pelion region and assigned top-SE and top-E tectonic transport to the Early Cretaceous. NW-SE and E-W trending stretching lineations have been determined in the Pelagonian unit in NW-Thessaly (Kilias et al., 1990; Sfeikos, 1992), and in the northern part of the Pelagonian zone (Kilias et al., 2010; Most, 2003; Sharp, 1994; Sharp & Robertson, 2006) without identifying a preferential sense of shear (Figure 10a). The above-mentioned ductile fabrics imply NW-SE or E-W tectonic transport and have been assigned to the Late Jurassic or Early Cretaceous ophiolite emplacement and subsequent deformation of the Pelagonian zone or alternatively to an early collision between Pelagonia and Rhodopia (Schenker et al., 2014).

Further to the NW, the Pelagonian zone continues in the Internal Dinarides. Based on stratigraphy and structural position, the Pelagonian zone of the Hellenides can clearly be correlated with the Internal Adria-derived thrust sheets structurally underlying the obducted ophiolites of the Dinarides (e.g., Schmid et al., 2008). Early Cretaceous metamorphism in the Internal Dinarides is constrained by K/Ar thermochronology (Milovanović, 1984; Milovanovic et al., 1995; Porkoláb et al., 2018; Tomljenović et al., 2008), and Early-to Late Cretaceous metamorphism by $^{40}Ar/^{39}Ar$ thermochronology (Schefer, 2012). Similar to the Pelagonian zone in the Hellenides, WNW-ESE stretching lineations and top-WNW sense of shear has been reported from the subophiolitic units marking the tectonic transport direction of the ophiolite thrust sheet(s;Carosi et al., 1996; Schefer, 2012; Schmid et al., 2008). Our correlation shows that Early Cretaceous tectono-metamorphic events along the Pelagonian zone in Greece and in the Internal Dinarides have similar timing and similar directions of tectonic transport following the emplacement of Neotethyan ophiolites.

6.2. Early Cretaceous Underthrusting of the Pelagonian Margin

Cessation of deposition on the Pelagonian margin is linked with the obduction of Neotethyan ophiolites (e.g., Danelian & Robertson, 2001; Scherreiks, 2000). Subduction initiated in an intraoceanic setting (e.g., Barth et al., 2008; Bortolotti et al., 2013; Maffione et al., 2015) in Middle-Late Jurassic times (Spray et al., 1984; Dimo-Lahitte et al., 2001; Figure 11a). As shown on Figure 10a and discussed in section 6.1, Early Cretaceous deformation and metamorphism can be correlated from Skopelos, through the Pelagonian zone, up to the Internal Dinarides. Consequently, underthrusting of the distal Pelagonian/Adriatic units below the obducting Neotethyan units was a regional-scale process. The thermo-mechanical feasibility of such a system has been tested numerically with a series of experiments, suggesting that ophiolite obduction is a process that remains stable in a broad physical parameter range (Duretz et al., 2016). Strong continental basement rheology plays a key role in obduction while switch from compression to extension seems to be important for the subsequent exhumation of metamorphic rocks following underthrusting (Duretz et al., 2016). However, the effect of surface processes on the conditions of exhumation has not been investigated yet, and the general lack of identified major Early Cretaceous exhuming structures (shear zones or normal faults) in the region might imply that erosion played a major role in this process. Exhumation following a short-lived underthrusting of the continental margin is consistent with the presence of regional Late Jurassic-Early Cretaceous unconformities truncating both oceanic and metamorphosed continental units (Jacobshagen & Wallbrecher, 1984; Robertson, 1991; Sharp, 1994) in the Pelagonian zone (Figure 11c). The trend of tectonic transport during the Late Jurassic-Early Cretaceous along the Pelagonian zone is consistently between NW-SE and E-W (Figure 10a) but kinematic indicators are observed to be double-vergent (both top-to-the-NW to W and top-to-the-SE to E) on Skopelos (Figure 3) as well as and on a larger scale (Figure 10a). According to plate tectonic reconstructions, the Pelagonian/Adriatic continental margin was located to the W (e.g., Maffione & van Hinsbergen, 2018; Robertson et al., 1996) or SW (e.g., Stampfli &

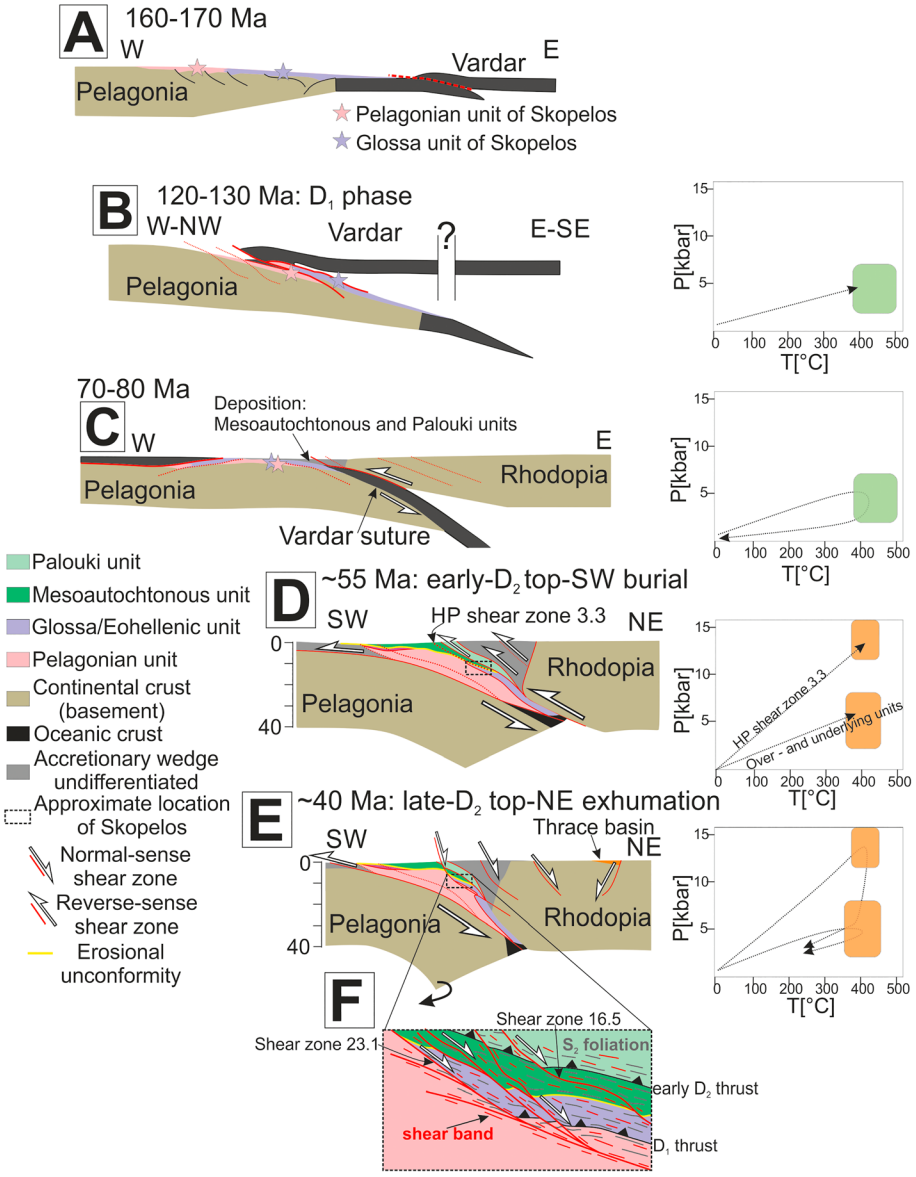

Figure 11. Simplified five-step evolutionary model of the Pelagonian margin and the tectonic units of Skopelos between ~170 and ~40 Ma. For steps b to e, plots show the estimated pressure-temperature evolution of Skopelos. (a) Intraoceanic subduction initiation in the proximity of the Pelagonian passive margin. (b) Underthrusting of the Pelagonian margin below the Vardar ophiolites driving metamorphism and deformation (D_1 on Skopelos) of the passive margin sediments. The Glossa unit is emplaced on top of the Pelagonian unit. (c) Uplift and erosion of the Pelagonian margin and the obducted ophiolites. Deposition of Late Cretaceous sediments (Mesoautochtonous and Palouki units on Skopelos) on top of the metamorphic rocks. (d) Development of an accretionary wedge in the collision zone between Pelagonia and Rhodopia. All the units of Skopelos were incorporated in the wedge after being carried down by the subducting Pelagonian basement. Top-to-the-SW tectonic transport and greenschist to blueschist facies metamorphism characterized the burial of the units. (e) Initial exhumation of the accretionary wedge by top-to-the-NE extensional shearing following the initiation of slab roll-back. (f) Magnification of the approximate location of Skopelos on Figure 11e showing the detailed interpretation of the observed pervasive top-to-the-NE shearing. The shear zones run subparallel to the main foliation (S_2) causing only minor modifications in the nappe structure but triggering the development of distributed top-to-the-NE shear in all the units of Skopelos.

Borel, 2002) from the Neotethys/Vardar oceanic domain. Considering that the clockwise rotation in the Pelagonian zone has been substantial (roughly 30-50°) since Eocene times (van Hinsbergen et al., 2008, and references therein; Hinsbergen & Schmid, 2012), we can restore the top-NW to W kinematic indicators to roughly top-to-the-W-SW. Therefore, in our view the Early Cretaceous top-to-the-NW-W

kinematic indicators (now in present-day coordinates) in the Pelagonian zone are likely to represent the record of underthrusting below the Neotethyan/Vardar ophiolites. This view is also supported by the top-to-the-W structural polarity of obduction-related deformation in Northeastern-Albania (Tremblay et al., 2015), in Western-Serbia (Porkoláb et al., 2018), and top-WNW shear sense indicators in the metamorphic sole and subophiolitic mélange of the Internal Dinarides (Carosi et al., 1996; Schmid et al., 2008; Schefer, 2012).

On the other hand, the interpretation of the commonly found opposite top-to-the-SE to E kinematic indicators within the Pelagonian zone (Figure 10a) remains enigmatic. A sound solution would be to assign the top-to-the-SE to E shearing to the extensional exhumation of the continental margin following the obduction of the ophiolites; however, no convincing structural analysis has been presented so far which would confirm the extensional nature of these structures or the relative timing with respect to the top-NW to W shearing. An alternative explanation could be a double-vergent thrusting scenario producing both top-to-the-NW to W and top-to-the-SE to E shear zones related to the inversion of the passive margin during/following obduction. Both ideas would need to be confirmed by a robust structural analysis from multiple locations along the Pelagonian zone.

7. Implications for the Late Cretaceous-Paleogene Tectonics of the Pelagonian Zone

7.1. Correlation of Late Cretaceous-Paleogene Tectonic Burial in the Aegean Region

Deposition of Albian-Turonian transgressive conglomerates, carbonates, and on top Turonian-Paleogene flysch marks Late Cretaceous-Paleogene transgression and the evolution of a foredeep basin between Pelagonia and Eurasia/Rhodopia (Jacobshagen & Wallbrecher, 1984; Matarangas, 1992). Latest Cretaceous-Paleogene metamorphism and top-to-the-SW thrusting directions have been reported from all over the Aegean region (Figure 10b) and also from the Dinarides (e.g., Schefer, 2012). Recent tectonic models of the Aegean region suggest NE-ward subduction of the Pelagonian continental lithosphere below Eurasia/Rhodopia following the final closure of the Vardar ocean (e.g., Brun et al., 2016; Jolivet & Brun, 2010; Ricou et al., 1998). NE-ward subduction led to the formation of top-to-the-SW shear fabric in the lower plate units such as Pelagonia associated with prograde metamorphism (Figure 10b; Philippon et al., 2011; Brun et al., 2016, and references therein). Lower plate units, which are now found on the surface, have experienced metamorphism in various degrees. Blueschist to greenschist facies rocks with Late Cretaceous-Early Eocene mylonitic fabrics are found in the tectonic windows of the Olympos and Ossa regions where a more external thrust sheet of the Hellenides-nappe-stack crop out (Schermer et al., 1990; Lips et al., 1998; Figure 1). Rocks from greenschist to blueschist facies are also found in the Pelion peninsula showing Paleogene-Miocene fabric ages (Gerogiannis & Xypolias, 2017; Lips et al., 1999; Walcott, 1998). Blueschist to eclogite facies rocks with Paleogene fabrics are found in the region of the Cyclades (e.g., Jolivet et al., 2010; Jolivet & Brun, 2010; Laurent et al., 2017; Lister & Forster, 2016; Wijbrans et al., 1990). Rb/Sr dating from the North Pelagonian zone has also indicated Paleogene metamorphism (Koroneos et al., 1993). All these results have been assigned to the Paleogene suturing of Adria-and Europe-derived units and the formation of the SW-verging Aegean nappe stack. Paleogene suturing of Adria-derived units and Eurasia is also well documented in the Internal Dinarides: top-to-the-SSW to W nappe stacking and related metamorphism has been dated and reported from the Kopaonik thrust sheet (Schefer, 2012) and the Sava Zone (Ustaszewski et al., 2010). Based on the Paleogene foredeep deposits of Skopelos (Mesoautchtonous and Palouki flysch formations) and the similarities in timing and kinematics of ductile deformation shown by Figure 10b, we correlate the top-SW D_2 structures of Skopelos and related S_2 fabric formation defined by the present study with the final closure of the Neotethys ocean that led to the second episode of burial and subsequent exhumation of the Pelagonian zone (Figure 11d).

7.2. Paleogene Accretionary Wedge Evolution on Skopelos

The metamorphic grade during D_2 phase was greenschist facies for all units of Skopelos, except for one blueschist facies shear zone (Figures 5a and 7) located at the base of the Mesoautochtonous unit. These findings are not consistent with reconstructions that incorporate the entire Northern Sporades in the belt of Aegean high-pressure rocks, which have been subducted to great depth in Paleogene times (e.g., Figure 4

in Brun et al., 2016). The grade of metamorphism is rather consistent with shallow tectonic processes in an accretionary wedge, which formed during the collision of Pelagonia and Rhodopia (Figure 11d).

The Mesoautochtonous unit and the upper formations of the Palouki unit were deposited in a convergent setting in front of the advancing thrusts of the Europe-derived units (Rhodopia; Figures 11c and 11d). The upper formations of the Palouki unit were deposited coevally but at distance from the equivalent Mesoautochtonous formations (Matarangas, 1992), which is also reflected in the slightly different heavy mineral composition of the two flysch successions (Faupl et al., 1999). Following deposition of the flysch formations, the Palouki unit was thrust on top of the Mesoautochtonous unit (Figures 11d). The Ar/Ar age of the mylonitic sericite fabric (S_2) in the Turonian-Paleogene flysch is roughly 53Ma (Figure 9). Consequently, the deposition of the Mesoautochtonous and the Palouki units ceased prior to the Paleocene-Eocene boundary, and the units were subsequently transported to a depth of greenschist facies conditions (roughly 10-15 km) together with the subducting Pelagonian basement. Greenschist facies conditions suggests that the Mesoautochtonous and the Palouki units were detached from the downgoing plate by a thrust system and were incorporated in the accretionary wedge, which was evolving on top of the downgoing plate (Figure 11d). Similar greenschist facies syn-D_2 metamorphic conditions of the Pelagonian and Glossa units as well as of the basal formation of the Palouki unit imply that these formations were also incorporated in the accretionary wedge instead of being subducted (Figure 11d). Ar/Ar fabric ages from the Pelagonian and Glossa units are somewhat (~10 Ma) older than the ones from the Mesoautochtonous unit (Figure 9) suggesting that these formations might have been buried earlier (latest Cretaceous-Early Paleocene), while the flysch units were still depositing in the foredeep basin. The partial activation of the erosional contact between the Mesoautochtonous and Pelagonian units (Figure 2, for details see section 5.2) as top-SW shear zone (Figure 11d) is easiest explained assuming that this originally erosional contact has been dipping in the same direction than the thrusts of the accretionary wedge (Figure 11d).

Pressure recorded within the mylonitic metapelites, exposed between the Pelagonian and the Mesoautochtonous units is significantly higher compared to the Mesoautochtonous unit above and to the Pelagonian unit below; these units have only experienced greenschist facies metamorphism (Figure 11d). Explanations for such pressure differences depend on the approach in converting pressure to depth. Traditionally, pressure as recorded by mineral assemblages is interpreted in terms of overburden (lithostatic) pressure (e.g., Jolivet et al., 2003), whereas other authors (e.g., Schmalholz & Podladchikov, 2013) suggest that tectonic overpressure may be significant in some instances. These fundamentally different ways of interpreting the meaning of pressure inevitably leads to substantially different tectonic interpretations of the same *P-T* path recorded by the metamorphic rocks. In our case assuming that the recorded pressure corresponds to the lithostatic pressure demands a complicated tectonic model: a thin slice of metapelites needs to be subducted to much greater depth with respect to the overlying and underlying units and subsequently exhumed in a way that accommodates a differential displacement and transports the blueschist-facies metapelites between the greenschist facies units. On the other hand, accounting for overpressure in the metapelites instead of assuming large differential displacements would provide a much simpler solution, which is also consistent with our observations. Numerical simulations of lithospheric shortening have demonstrated that pressure can significantly increase inside weak crustal shear zones (such as the one between the Pelagonian and the Mesoautochtonous units) to maintain a constant depth-averaged horizontal total stress and to fulfill the horizontal force balance across the shear zone (Moulas et al., 2014; Schmalholz & Podladchikov, 2013). Thus, we suggest that the high-pressure assemblage on Skopelos could be an example where tectonic overpressure inside a prograde, greenshist facies, weak shear zone has led to aerially restricted blueshist facies metamorphism related to top WSW shearing at the tectonic contact between the Pelagonian and the Mesoautochtonous units (Figure 11d).

7.3. Top-NE Exhumation of the Accretionary Wedge

The simultaneous onset of exhumation and extension in the Aegean region suggests that these processes are intimately linked (Brun et al., 2016; Brun & Sokoutis, 2007, 2010). The switch from contraction to extension is commonly related to the subduction of buoyant continental block(s) and resulting initiation of slab-rollback during the Eocene (Brun & Faccenna, 2008). Slab-rollback resulted in trench retreat and related NE-SW extension in the upper plate. Top-NE shear zones localized in the Pelagonian zone (Figure 10b), top-to-the-NE regional detachment(s) in the Northern Cyclades (Gautier & Brun, 1994; Grasemann et al.,

2012; Jolivet et al., 2010), and a top-to-the-SW regional detachment in Southern Rhodopia (Brun & Sokoutis, 2007; Dinter & Royden, 1993).

We correlate the top-to-the-NE ductile deformation of Skopelos with the early-stage exhumation of the Late-Cretaceous-Paleogene accretionary wedge. Our observations (Figure 3b) are consistent with the commonly observed top-to-the-NE exhumation in the Aegean region (Figure 10b; Brun et al., 2016, and references therein). Latest Cretaceous-earliest Eocene S_2 mylonitic fabrics (Figure 9) most likely formed during the tectonic burial of the rocks, setting an Early Eocene upper boundary for the possible onset of exhumation in case of Skopelos. This upper boundary is consistent with the 40-45 Ma onset of exhumation in Rhodopia (Brun & Sokoutis, 2007; Lips et al., 2000) and in the Ossa-Olympos-region (Lips et al., 1998; Schermer et al., 1990; Walcott, 1998). Younger, Eocene to Oligocene onset of exhumation has been inferred for the Pelion peninsula (Lips et al., 1999) as well as for the Cyclades (Brun et al., 2016; Jolivet et al., 2010; Jolivet & Brun, 2010; Lister & Forster, 2016; Uunk et al., 2018; Wijbrans et al., 1990) supporting the hypothesis that the southward migration of extensional and compressional domains was coupled to trench retreat leading to the southward decreasing age of exhumation (Jolivet & Brun, 2010).

Apatite fission track data (Hejl et al., 1999) suggest that the rocks of Skopelos have already been exhumed to a near-surface position by mid-Oligocene times. This implies that most of the exhumation took place between the late-Eocene and early-Oligocene. The ductile stage of exhumation on Skopelos was accommodated by small to medium-sized, top-to-the-NE shear zones and distributed top-to-the-NE shearing between the main structures (Figure 11f). The exact amount of exhumation accommodated by these structures remains uncertain, but could be quantified in the future with the specific dating of exhumation-related fabrics and zircon fission track dating. Later normal faulting is probably linked with the evolution of the North Aegean Trough, and is also likely to have played a significant role during final exhumation of the rocks to the surface.

8. Conclusions

The coupled application of multiscale structural analysis, metamorphic petrology, and white mica $^{40}Ar/^{39}Ar$ dating allowed to define two distinct episodes of tectonic burial and exhumation on the island of Skopelos.

Early Cretaceous (~105-135Ma) tectonic burial and exhumation affected the Pelagonian, Glossa, and the lowermost formation of the Palouki units and developed a first generation of isoclinal folds (F_1) and a related foliation (S_1). We correlate the top-to-the-NW and top-SE shearing and greenschist facies metamorphism of D_1 with the underthrusting of the Pelagonian or Adriatic margin below the Vardar ophiolites. The structural and geochronological record of this underthrusting can be correlated up to the Internal Dinarides.

Underthrusting was followed by exhumation and erosion of the Pelagonian margin. The exhumation of the Pelagonian, Glossa, and the lowermost formation of the Palouki units of Skopelos took place during the late Early Cretaceous and were subsequently transgressed by the younger sedimentary sequences from the latest Albian-Early Cenomanian (~100-95 Ma).

Latest Cretaceous-Early Eocene $^{40}Ar/^{39}Ar$ white mica ages of mylonitic S_2 foliations attest to a second phase of burial and exhumation of Skopelos. A second generation of isoclinal folds (F_2) and tectonic foliation (S_2) developed during top-to-the-SW and following top-to-the-NE shearing under greenschist facies conditions.

The Late Cretaceous-Paleogene sedimentary cycle exposed on Skopelos was deposited in a compressional setting and was buried during subduction of the Pelagonian basement to greenschist facies conditions.

We propose that all the rocks of Skopelos were detached from the downgoing Pelagonian basement by top-to-the-SW thrusts and incorporated in an accretionary wedge that evolved above the downgoing plate during Paleogene times. Top-to-the-SW shear fabrics formed during the tectonic burial of the rocks, while opposite top-to-the-NE fabrics formed during the first stage of extensional exhumation.

A shear zone in Al-rich metapelites records significantly higher pressure than the overlying Mesoautochtonous and the underlying Pelagonian units. In our view the pressure difference could be an example of tectonic overpressure inside a prograde, weak shear zone.

Appendix

The Appendix contains mineral analyses data (A1) and whole-rock composition data (A2) of sample 3.3, as well as the description and location of samples selected for Ar/Ar dating (A3).

Table A1
Representative Mineral Analyses of Sample 3.3

Phase	Phengite			Chloritoid		Carpholite	Hematite
Notes	matrix	syn-pc	syn-pr	pre-pc	pre-pr	incl. in ctd	matrix
wt.% oxides							
SiO_2	46.9	24.03	24.74	25.04	25.29	36.45	
TiO2							0.86
$A1_2O_3$	36.02	40.87	41.64	41.74	42.03	33.14	
Fe_2O_3							96.56
FeO	2.11	18.16	17.81	19.39	18.09	10.32	
MnO		6.75	5.57	7.01	6.52	0.98	0.56
MgO	0.7	2.59	3.2	2.47	2.89	5.67	
K_2O	9.6						
Na_2O	0.56						
Total	95.89	92.4	92.96	95.65	94.82	86.56	97.98
Cations							
Si	3.09	1.99	2.01	2.01	2.03	1.95	
Ti							0.02
Al	2.8	3.98	3.99	3.94	3.97	2.09	
Fe3+							1.97
Fe2+	0.12	1.26	1.21	1.3	1.21	0.46	
Mn		0.47	0.38	0.48	0.44	0.04	0.01
Mg	0.07	0.32	0.39	0.3	0.35	0.45	
K	0.81						
Na	0.07						
Total	6.95	8.02	7.99	8.02	7.99	5	2
Mg#	0.368	0.203	0.244	0.188	0.224	0.495	
Oxygens	11	12	12	12	12	8	3

Abbreviations: Syn, syn-mylonitic; pre, pre-mylonitic; pc, porphyroblast core; pr, porphyroblast rim.

Table A2
Whole-Rock Composition of Sample 3.3

wt.%	
SiO_2	62.66
TiO_2	0.99
Al_2O_3	20.21
FeO	5.49
MnO	0.55
MgO	1.11
CaO	0.31
Na_2O	0.31
K_2O	4.79
P_2O_5	0.02
LOI	3.56
Total	100.00

Table A3
Location and Description of Dated Samples

No.	Lat	Lon	Method	Unit	Description
1.2	39.164	23.627	single grain	Glossa	brown schistose metasandstone with metaconglomerate layers
7.3	39.163	23.640	single grain	Pelagonian	grey phyllitic schist
8.1	39.174	23.650	single grain	Pelagonian	heavily deformed light brown pyhillite with metasandstone layers
12.4	39.087	23.754	single grain	M Flysch	grey metasandstone with large detrital white micas
13.2	39.104	23.741	single grain	P Flysch	brown phyllite with large detrital white micas
13.6	39.128	23.710	single grain	M Flysch	brown phyllite with coarser metasandstone layers
17.5	39.124	23.758	single grain	P Flysch	brown phyllite with large detrital white micas
2.2	39.176	23.634	fabric	Glossa	brown phyllitic schist with well-developed S2 sericitic foliation
3.3	39.128	23.677	fabric	M Metapelites	purple to grey metapelites with mylonitic S2 foliation
7.1	39.165	23.634	fabric	Pelagonian	grey phyllitic schist with well-developed S1 and S2 foliations
7.2	39.167	23.635	fabric	Glossa	grey to light pink phyllitic schist
12.3	39.085	23.753	fabric	M Flysch	grey phyllite with well-developed S2 sericitic foliation

Abbreviations: No., sample number; Lat, latitude; Lon, longitude; M, mesoautochtonous; P, Palouki.

Acknowledgments
The research leading to these results has received funding from the European Union's MSCA-ITN-ETN Project SUBITOP 674899. $^{40}Ar/^{39}Ar$ dating was performed in collaboration with the VU University Amsterdam, while pressure-temperature calculations and microprobe analysis in collaboration with the National and Kapodistrian University of Athens. We thank to the reviewers and editors for substantially improving our manuscript with their constructive remarks. We also thank to Evangelos Moulas for his helpful advices regarding pressure-temperature calculations and Jean-Pierre Brun for fruitful discussions on the Aegean geology. The data supporting this paper are available from the Utrecht University Tectonics database via uu.teclab@gmail.com.

References

Agard, P., Jolivet, L., & Goffe, B. (2001). Tectonometamorphic evolution of the Schistes Lustres Complex; Implications for the exhumation of HP and UHP rocks in the Western Alps. *Bulletin de la Société géologique de France*, *172*(5), 617–636. https://doi.org/10.2113/172.5.617

Altherr, R., Schliestedt, M., Okrusch, M., Seidel, E., Kreuzer, H., Harre, W., et al. (1979). Geochronology of high-pressure rocks on Sifnos (Cyclades, Greece). *Contributions to Mineralogy and Petrology*, *70*(3), 245–255. https://doi.org/10.1007/BF00375354

Aubouin, J., Bonneau, M., Davidson, J., Leboulenger, P., Matesco, S., & Zambetakis, A. (1976). Esquisse structurale de l9Arc egeen externe; des Dinarides aux Taurides. *Bulletin de la Societé géologique de France*, *7*(2), 327–336.

Barth, M. G., Mason, P. R., Davies, G. R., & Drury, M. R. (2008). The Othris Ophiolite, Greece: a snapshot of subduction initiation at a mid-ocean ridge. *Lithos*, *100*(1-4), 234–254. https://doi.org/10.1016/j.lithos.2007.06.018

Beltrando, M., Lister, G. S., Forster, M., Dunlap, W. J., Fraser, G., & Hermann, J. (2009). Dating microstructures by the 40Ar/39Ar step-heating technique: Deformation–pressure–temperature–time history of the Penninic Units of the Western Alps. *Lithos*, *113*(3-4), 801–819. https://doi.org/10.1016/j.lithos.2009.07.006

Blake, M., Bonneau, M., Geyssant, J., Kienast, J., Lepvrier, C., Maluski, H., & Papanikolaou, D. (1981). A geologic reconnaissance of the Cycladic blueschist belt, Greece. *Geological Society of America Bulletin*, *92*(5), 247–254. https://doi.org/10.1130/0016-7606(1981)92<247:AGROTC>2.0.CO;2

Bortolotti, V., Chiari, M., Marroni, M., Pandolfi, L., Principi, G., & Saccani, E. (2013). Geodynamic evolution of ophiolites from Albania and Greece (Dinaric-Hellenic belt): One, two, or more oceanic basins? *International Journal of Earth Sciences*, *102*(3), 783–811. https://doi.org/10.1007/s00531-012-0835-7

Bortolotti, V., Marroni, M., Pandolfi, L., & Principi, G. (2005). Mesozoic to Tertiary tectonic history of the Mirdita ophiolites, northern Albania. *Island Arc*, *14*(4), 471–493. https://doi.org/10.1111/j.1440-1738.2005.00479.x

Bortolotti, V., & Principi, G. (2005). Tethyan ophiolites and Pangea break-up. *Island Arc*, *14*(4), 442–470. https://doi.org/10.1111/j.1440-1738.2005.00478.x

Bröcker, M., Baldwin, S., & Arkudas, R. (2013). The geological significance of 40Ar/39Ar and Rb–Sr white mica ages from Syros and Sifnos, Greece: A record of continuous (re) crystallization during exhumation? *Journal of Metamorphic Geology*, *31*(6), 629–646. https://doi.org/10.1111/jmg.12037

Bröcker, M., Kreuzer, H., Matthews, A., & Okrusch, M. (1993). 40Ar/39Ar and oxygen isotope studies of polymetamorphism from Tinos Island, Cycladic blueschist belt, Greece. *Journal of Metamorphic Geology*, *11*(2), 223–240. https://doi.org/10.1111/j.1525-1314.1993.tb00144.x

Brun, J.-P., & Faccenna, C. (2008). Exhumation of high-pressure rocks driven by slab rollback. *Earth and Planetary Science Letters*, *272*(1-2), 1–7. https://doi.org/10.1016/j.epsl.2008.02.038

Brun, J.-P., Faccenna, C., Gueydan, F., Sokoutis, D., Philippon, M., Kydonakis, K., & Gorini, C. (2016). The two-stage Aegean extension, from localized to distributed, a result of slab rollback acceleration 1. *Canadian Journal of Earth Sciences*, *53*(11), 1142–1157. https://doi.org/10.1139/cjes-2015-0203

Brun, J.-P., & Sokoutis, D. (2007). Kinematics of the southern Rhodope core complex (North Greece). *International Journal of Earth Sciences*, *96*(6), 1079–1099. https://doi.org/10.1007/s00531-007-0174-2

Brun, J.-P., & Sokoutis, D. (2010). 45 my of Aegean crust and mantle flow driven by trench retreat. *Geology*, *38*(9), 815–818. https://doi.org/10.1130/G30950.1

Burg, J.-P. (2012). Rhodope: From Mesozoic convergence to Cenozoic extension. *Journal of the Virtual Explorer*, *42*, 1.

Carosi, R., Cortesogno, L., Gaggero, L. t., & Marroni, M. (1996). Geological and petrological features of the metamorphic sole from the Mirdita nappe, northern Albania. *Ofioliti*, *21*(1), 21–40.

Clift, P. D., & Dixon, J. (1998). Jurassic ridge collapse, subduction initiation and ophiolite obduction in the southern Greek Tethys. *Eclogae Geologicae Helvetiae*, *91*, 123–138.

Connolly, J. (2009). The geodynamic equation of state: What and how. *Geochemistry, Geophysics, Geosystems*, *10*, Q10014. https://doi.org/10.1029/2009GC002540

Connolly, J. A. (2005). Computation of phase equilibria by linear programming: A tool for geodynamic modeling and its application to subduction zone decarbonation. *Earth and Planetary Science Letters*, *236*(1-2), 524–541. https://doi.org/10.1016/j.epsl.2005.04.033

Danelian, T., & Robertson, A. H. (2001). Neotethyan evolution of eastern Greece (Pagondas Melange, Evia island) inferred from radiolarian biostratigraphy and the geochemistry of associated extrusive rocks. *Geological Magazine*, *138*(3), 345–363. https://doi.org/10.1017/S0016756801005337

De Bono, A. (1998). Pelagonian Margins in central Evia island (Greece): stratigraphy and geodynamic evolution, Université de Lausanne.
De Bono, A., Martini, R., Zaninetti, L., Hirsch, F., Stampfli, G. M., & Vavassis, I. (2001). Permo-Triassic stratigraphy of the pelagonian zone in central Evia island (Greece). *Eclogae Geologicae Helvetiae*, *94*, 289–311.
Dilek, Y., Furnes, H., & Shallo, M. (2007). Suprasubduction zone ophiolite formation along the periphery of Mesozoic Gondwana. *Gondwana Research*, *11*(4), 453–475. https://doi.org/10.1016/j.gr.2007.01.005
Dimo-Lahitte, A., Monié, P., & Vergély, P. (2001). Metamorphic soles from the Albanian ophiolites: Petrology, 40Ar/39Ar geochronology, and geodynamic evolution. *Tectonics*, *20*(1), 78–96. https://doi.org/10.1029/2000TC900024
Dinter, D. A., & Royden, L. (1993). Late Cenozoic extension in northeastern Greece: Strymon Valley detachment system and Rhodope metamorphic core complex. *Geology*, *21*(1), 45–48. https://doi.org/10.1130/0091-7613(1993)021<0045:LCEING>2.3.CO;2
Duretz, T., Agard, P., Yamato, P., Ducassou, C., Burov, E. B., & Gerya, T. V. (2016). Thermo-mechanical modeling of the obduction process based on the Oman ophiolite case. *Gondwana Research*, *32*, 1–10. https://doi.org/10.1016/j.gr.2015.02.002
Faupl, P., Pavlopoulos, A., & Migiros, G. (1999). The Paleogene history of the Pelagonian zone SL (Hellenides, Greece): Heavy mineral study from terrigenous flysch sediments. *Geologica Carpathica*, *50*(6), 449–458.
Gautier, P., & Brun, J.-P. (1994). Crustal-scale geometry and kinematics of late-orogenic extension in the central Aegean (Cyclades and Ewia Island). *Tectonophysics*, *238*(1-4), 399–424. https://doi.org/10.1016/0040-1951(94)90066-3
Gawlick, H.-J., Sudar, M., Suzuki, H., Deric, N., Missoni, S., Lein, R., & Jovanović, D. (2009). Upper Triassic and Middle Jurassic radiolarians from the ophiolitic mélange of the Dinaridic Ophiolite Belt, SW Serbia. *Neues Jahrbuch für Geologie und Paläontologie (Abhandlungen)*, *253*(2), 293–311. https://doi.org/10.1127/0077-7749/2009/0253-0293
Gerogiannis, N., & Xypolias, P. (2017). Retroward extrusion of high-pressure rocks: An example from the Hellenides (Pelion Blueschist Nappe, NW Aegean). *Terra Nova*, *29*(6), 372–381. https://doi.org/10.1111/ter.12297
Goffé, B., Goffé-Urbano, G., & Saliot, P. (1973). Sur la présence d'une variété magnésienne de la ferrocarpholite en Vanoise (Alpes françaises): sa signification probable dans le métamorphisme alpin. *Comptes Rendus de l'Académie des Sciences Paris*, *277*, 1965–1968.
Goffé, B., Michard, A., Kienast, J. R., & Le Mer, O. (1988). A case of obduction-related high-pressure, low-temperature metamorphism in upper crustal nappes, Arabian continental margin, Oman: PT paths and kinematic interpretation. *Tectonophysics*, *151*(1-4), 363–386. https://doi.org/10.1016/0040-1951(88)90253-3
Grasemann, B., Schneider, D. A., Stöckli, D. F., & Iglseder, C. (2012). Miocene bivergent crustal extension in the Aegean: Evidence from the western Cyclades (Greece). *Lithosphere*, *4*(1), 23–39. https://doi.org/10.1130/L164.1
Hejl, E., Riedl, H., & Weingartner, H. (1999). Cretaceous palaeokarst and Cenozoic erosion of the North Sporades (Greece): Results from geomorphological studies and fission-track analysis. *Mitttheilungen der Österreichischen Geologischen Gesellschaft*, *90*, 67–82.
Hinsbergen, D. J., & Schmid, S. M. (2012). Map view restoration of Aegean–West Anatolian accretion and extension since the Eocene. *Tectonics*, *31*, TC5005. https://doi.org/10.1029/2012TC003132
Hunziker, D., Burg, J. P., Moulas, E., Reusser, E., & Omrani, J. (2017). Formation and preservation of fresh lawsonite: Geothermobarometry of the North Makran Blueschists, southeast Iran. *Journal of Metamorphic Geology*, *35*(8), 871–895.
Jacobshagen, V., & Matarangas, D. (2004). Nappe structure of the North Sporades (Greece): on the geological evolution of Alonnisos Island. *Δελτίον της Ελληνικής Γεωλογικής Εταιρίας*, *36*(4), 1636–1642.
Jacobshagen, V., Skala, W., & Wallbrecher, E. (1978). Alpine structure and development of the southern Pelion peninsula and the North Sporades. *Alps, Apennines, Hellenides Sci Report*, *38*, 484–488.
Jacobshagen, V., & Wallbrecher, E. (1984). Pre-Neogene nappe structure and metamorphism of the North Sporades and the southern Pelion peninsula. *Geological Society, London, Special Publications*, *17*(1), 591–602. https://doi.org/10.1144/GSL.SP.1984.017.01.46
Jolivet, L., & Brun, J.-P. (2010). Cenozoic geodynamic evolution of the Aegean. *International Journal of Earth Sciences*, *99*(1), 109–138. https://doi.org/10.1007/s00531-008-0366-4
Jolivet, L., Faccenna, C., Goffé, B., Burov, E., & Agard, P. (2003). Subduction tectonics and exhumation of high-pressure metamorphic rocks in the Mediterranean orogens. *American Journal of Science*, *303*(5), 353–409. https://doi.org/10.2475/ajs.303.5.353
Jolivet, L., Lecomte, E., Huet, B., Denèle, Y., Lacombe, O., Labrousse, L., et al. (2010). The north cycladic detachment system. *Earth and Planetary Science Letters*, *289*(1-2), 87–104. https://doi.org/10.1016/j.epsl.2009.10.032
Kelepertsis, A. (1974). Geological structure of Alonnisos and Peristera islands (Aegaean Sea, Greece). *Zeitschrift der Deutschen Geologischen Gesellschaft*, 225–236.
Kilias, A., Frisch, W., Avgerinas, A., Dunkl, I., Falalakis, G., & Gawlick, H.-J. (2010). Alpine architecture and kinematics of deformation of the northern Pelagonian nappe pile in the Hellenides. *Austrian Journal of Earth Sciences*, *103*, 4–28.
Kilias, A., Kasselas, G., & Nastos, G. (1990). Quartz c-axis fabrics as a kinematic indicator of sense of nappe emplacement—an example from the NE Pieria mountain area (Greece). *Zeitschrift für Angewandte Geologische*, *36*(11), 427–433.
Koppers, A. A. (2002). ArArCALC—software for 40 Ar/39 Ar age calculations. *Computers & Geosciences*, *28*(5), 605–619. https://doi.org/10.1016/S0098-3004(01)00095-4
Koroneos, A., Christofides, G., Del Moro, A., & Kilias, A. (1993). Rb-Sr geochronology and geochemical aspects of the Eastern Varnountas plutonite (NW Macedonia, Greece). *Neues Jahrbuch für Mineralogie, Abhandlungen*, *165*(3), 297–315.
Kuiper, K., Deino, A., Hilgen, F., Krijgsman, W., Renne, P., & Wijbrans, J. R. (2008). Synchronizing rock clocks of Earth history. *Science*, *320*(5875), 500–504. https://doi.org/10.1126/science.1154339
Kydonakis, K., Brun, J.-P., Poujol, M., Monié, P., & Chatzitheodoridis, E. (2016). Inferences on the Mesozoic evolution of the North Aegean from the isotopic record of the Chalkidiki block. *Tectonophysics*, *682*, 65–84. https://doi.org/10.1016/j.tecto.2016.06.006
Laurent, V., Huet, B., Labrousse, L., Jolivet, L., Monie, P., & Augier, R. (2017). Extraneous argon in high-pressure metamorphic rocks: Distribution, origin and transport in the Cycladic Blueschist Unit (Greece). *Lithos*, *272*, 315–335.
Liati, A., Gebauer, D., & Fanning, C. M. (2004). The age of ophiolitic rocks of the Hellenides (Vourinos, Pindos, Crete): First U–Pb ion microprobe (SHRIMP) zircon ages. *Chemical Geology*, *207*(3-4), 171–188. https://doi.org/10.1016/j.chemgeo.2004.02.010
Lips, A., White, S., & Wijbrans, J. (1998). 40 Ar/39 Ar laserprobe direct dating of discrete deformational events: a continuous record of early Alpine tectonics in the Pelagonian Zone, NW Aegean area, Greece. *Tectonophysics*, *298*(1-3), 133–153. https://doi.org/10.1016/S0040-1951(98)00181-4
Lips, A., Wijbrans, J., & White, S. (1999). New insights from 40Ar/39Ar laserprobe dating of white mica fabrics from the Pelion Massif, Pelagonian Zone, Internal Hellenides, Greece: Implications for the timing of metamorphic episodes and tectonic events in the Aegean region. *Geological Society, London, Special Publications*, *156*(1), 457–474. https://doi.org/10.1144/GSL.SP.1999.156.01.21
Lips, A. L., White, S. H., & Wijbrans, J. R. (2000). Middle-late Alpine thermotectonic evolution of the southern Rhodope Massif, Greece. *Geodinamica Acta*, *13*(5), 281–292. https://doi.org/10.1080/09853111.2000.11105375

Lister, G., & Forster, M. (2016). White mica 40Ar/39Ar age spectra and the timing of multiple episodes of high-P metamorphic mineral growth in the Cycladic eclogite–blueschist belt, Syros, Aegean Sea, Greece. *Journal of Metamorphic Geology*, *34*(5), 401–421. https://doi.org/10.1111/jmg.12178

Maffione, M., Thieulot, C., Van Hinsbergen, D. J., Morris, A., Plümper, O., & Spakman, W. (2015). Dynamics of intraoceanic subduction initiation: 1. Oceanic detachment fault inversion and the formation of supra-subduction zone ophiolites. *Geochemistry, Geophysics, Geosystems*, *16*, 1753–1770. https://doi.org/10.1002/2015GC005746

Maffione, M., & van Hinsbergen, D. J. (2018). Reconstructing plate boundaries in the Jurassic neo-Tethys from the east and west Vardar ophiolites (Greece and Serbia). *Tectonics*, *37*, 858–887. https://doi.org/10.1002/2017TC004790

Matarangas, D. (1992). Geological investigation of Skopelos island, North Sporades, Greece, Forschungszentrum Jülich, Zentralbibliothek.

Mercier, J., Vergely, P., & Bebien, J. (1975). Les ophiolites helléniques «obductées» au Jurassique supérieur sont-elles les vestiges d'un Océan téthysien ou d'une mer marginale périeuropéenne. *Comptes Rendes Sommaires de la Société Géologique de France*, *17*, 108–111.

Milovanović, D. (1984). Petrology of low metamorphosed rocks of the central part of the Drina-Ivanjica Paleozoic. *Bulletin du Museum d'histoire Naturelle de Belgrade, A*, *39*, 13–139.

Milovanovic, D., Marchig, V., & Stevan, K. (1995). Petrology of the crossite schist from Fruška Gora Mts (Yugoslavia), relic of a subducted slab of the Tethyan oceanic crust. *Journal of Geodynamics*, *20*(3), 289–304. https://doi.org/10.1016/0264-3707(95)00005-T

Most, T. (2003). Geodynamic evolution of the Eastern Pelagonian Zone in northwestern Greece and the Republic of Macedonia. *Implications from U/Pb, Rb/Sr, K/Ar, Ar/Ar, geochronology and fission track thermochronology. Tubingen, Phd, Germany*, 1-170.

Moulas, E., Burg, J.-P., & Podladchikov, Y. (2014). Stress field associated with elliptical inclusions in a deforming matrix: mathematical model and implications for tectonic overpressure in the lithosphere. *Tectonophysics*, *631*, 37–49. https://doi.org/10.1016/j.tecto.2014.05.004

Moulas, E., Podladchikov, Y., Aranovich, L. Y., & Kostopoulos, D. (2013). The problem of depth in geology: When pressure does not translate into depth. *Petrology*, *21*(6), 527–538. https://doi.org/10.1134/S0869591113060052

Moulas, E., Schmalholz, S. M., Podladchikov, Y., Tajčmanová, L., Kostopoulos, D., & Baumgartner, L. (2018). Relation between mean stress, thermodynamic, and lithostatic pressure. *Journal of Metamorphic Geology*.

Mposkos, E., & Liati, A. (1991). Fe-carpholite in chloritoid-bearing metapelites–metasandstones of Skopelos Island, N. Sporades, Greece, paper presented at 5th Congress of the Geological Society of Greece. Deltio tes Ellenikes Geologikes Etaireias (Bulletin of the Geological Society of Greece).

Oberhänsli, R., Goffe, B., Jolivet, L., & Vidal, O. (1998). High-pressure–low-temperature metamorphism and deformation in the Bündnerschiefer of the Engadine window: Implications for the regional evolution of the eastern Central Alps. *Journal of Metamorphic Geology*, *16*(5), 657–674.

Pascual, F. J. R., Arenas, R., Catalán, J. R. M., Fernández, L. R. R., & Wijbrans, J. R. (2013). Thickening and exhumation of the Variscan roots in the Iberian Central System: Tectonothermal processes and 40Ar/39Ar ages. *Tectonophysics*, *587*, 207–221. https://doi.org/10.1016/j.tecto.2012.10.005

Passchier, C. W., & Trouw, R. A. (1996). *Microtectonics*. Berlin: Springer.

Philippon, M., Brun, J. P., & Gueydan, F. (2011). Tectonics of the Syros blueschists (Cyclades, Greece): From subduction to Aegean extension. *Tectonics*, *30*, TC4001. https://doi.org/10.1029/2010TC002810

Plunder, A., Agard, P., Chopin, C., & Okay, A. (2013). Tectono-metamorphic evolution of the Tavsanli zone, Western Anatolia: Implications for mechanical coupling during subduction/obduction processes, paper presented at EGU General Assembly Conference Abstracts.

Porkoláb, K., Kövér, S., Benkó, Z., Héja, G. H., Fialowski, M., Soós, B., et al. (2018). Structural and geochronological constraints from the Drina-Ivanjica thrust sheet (Western Serbia): Implications for the Cretaceous–Paleogene tectonics of the Internal Dinarides. *Swiss Journal of Geosciences*, 1–18.

Pourteau, A., Bousquet, R., Vidal, O., Plunder, A., Duesterhoeft, E., Candan, O., & Oberhänsli, R. (2014). Multistage growth of Fe–Mg–carpholite and Fe–Mg–chloritoid, from field evidence to thermodynamic modelling. *Contributions to Mineralogy and Petrology*, *168*(6), 1090. https://doi.org/10.1007/s00410-014-1090-7

Ricou, L.-E., Burg, J.-P., Godfriaux, I., & Ivanov, Z. (1998). Rhodope and Vardar: the metamorphic and the olistostromic paired belts related to the Cretaceous subduction under Europe. *Geodinamica Acta*, *11*(6), 285–309. https://doi.org/10.1080/09853111.1998.11105326

Robertson, A. (1991). Origin and emplacement of an inferred Late Jurassic subduction-accretion complex, Euboea, eastern Greece. *Geological Magazine*, *128*(1), 27–41. https://doi.org/10.1017/S0016756800018021

Robertson, A. (2004). Development of concepts concerning the genesis and emplacement of Tethyan ophiolites in the Eastern Mediterranean and Oman regions. *Earth-Science Reviews*, *66*(3-4), 331–387. https://doi.org/10.1016/j.earscirev.2004.01.005

Robertson, J., Dixon, S., Brown, A., Collins, A., Morris, E., Pickett, I. S., & Ustaömer, T. (1996). Alternative tectonic models for the Late Palaeozoic-Early Tertiary development of Tethys in the Eastern Mediterranean region. *Geological Society, London, Special Publications*, *105*(1), 239–263. https://doi.org/10.1144/GSL.SP.1996.105.01.22

Ryan, W. B., Carbotte, S. M., Coplan, J. O., O'Hara, S., Melkonian, A., Arko, R., et al. (2009). Global multi-resolution topography synthesis. *Geochemistry, Geophysics, Geosystems*, *10*, Q03014. https://doi.org/10.1029/2008GC002332

Schefer, S. (2012). Tectono-metamorphic and magmatic evolution of the Internal Dinarides (Kopaonik area, southern Serbia) and its significance for the geodynamic evolution of the Balkan Peninsula, University of Basel.

Schenker, F. L., Burg, J. P., Kostopoulos, D., Moulas, E., Larionov, A., & Quadt, A. (2014). From Mesoproterozoic magmatism to collisional Cretaceous anatexis: Tectonomagmatic history of the Pelagonian Zone, Greece. *Tectonics*, *33*, 1552–1576. https://doi.org/10.1002/2014TC003563

Schermer, E. R., Lux, D. R., & Burchfiel, B. C. (1990). Temperature-time history of subducted continental crust, Mount Olympos Region, Greece. *Tectonics*, *9*(5), 1165–1195. https://doi.org/10.1029/TC009i005p01165

Scherreiks, R. (2000). Platform margin and oceanic sedimentation in a divergent and convergent plate setting (Jurassic, Pelagonian Zone, NE Evvoia, Greece). *International Journal of Earth Sciences*, *89*(1), 90–107. https://doi.org/10.1007/s005310050319

Scherreiks, R., Bosence, D., BouDagher-Fadel, M., Meléndez, G., & Baumgartner, P. O. (2010). Evolution of the Pelagonian carbonate platform complex and the adjacent oceanic realm in response to plate tectonic forcing (Late Triassic and Jurassic), Evvoia, Greece. *International Journal of Earth Sciences*, *99*(6), 1317–1334. https://doi.org/10.1007/s00531-009-0461-1

Schmalholz, S. M., & Podladchikov, Y. Y. (2013). Tectonic overpressure in weak crustal-scale shear zones and implications for the exhumation of high-pressure rocks. *Geophysical Research Letters*, *40*, 1984–1988. https://doi.org/10.1002/grl.50417

Schmid, S. M., Bernoulli, D., Fügenschuh, B., Matenco, L., Schefer, S., Schuster, R., et al. (2008). The Alpine-Carpathian-Dinaridic orogenic system: correlation and evolution of tectonic units. *Swiss Journal of Geosciences*, *101*(1), 139–183. https://doi.org/10.1007/s00015-008-1247-3

Schneider, B., Kuiper, K., Postma, O., & Wijbrans, J. (2009). 40Ar/39Ar geochronology using a quadrupole mass spectrometer. *Quaternary Geochronology*, *4*(6), 508–516. https://doi.org/10.1016/j.quageo.2009.08.003

Sfeikos, A. (1992). Analysis of deformation and kinematics of the Pelagonian nappe system, Kamvounia mountains (North Thessaly, Greece), Thesis, University of Tubingen.

Sharp, I. R. (1994). The Triassic to Tertiary sedimentary, tectonic and magmatic evolution of the Pelagonian and Vardar (Axios) zones, Macedonia, Northern Greece, University of Edinburgh.

Sharp, I. R., & Robertson, A. H. (2006). Tectonic-sedimentary evolution of the western margin of the Mesozoic Vardar Ocean: Evidence from the Pelagonian and Almopias zones, northern Greece. *Geological Society, London, Special Publications*, *260*(1), 373–412. https://doi.org/10.1144/GSL.SP.2006.260.01.16

Simpson, C., & Schmid, S. M. (1983). An evaluation of criteria to deduce the sense of movement in sheared rocks. *Geological Society of America Bulletin*, *94*(11), 1281–1288. https://doi.org/10.1130/0016-7606(1983)94<1281:AEOCTD>2.0.CO;2

Spray, J., Bébien, J., Rex, D., & Roddick, J. (1984). Age constraints on the igneous and metamorphic evolution of the Hellenic-Dinaric ophiolites. *Geological Society, London, Special Publications*, *17*(1), 619–627. https://doi.org/10.1144/GSL.SP.1984.017.01.48

Stampfli, G. M., & Borel, G. (2002). A plate tectonic model for the Paleozoic and Mesozoic constrained by dynamic plate boundaries and restored synthetic oceanic isochrons. *Earth and Planetary Science Letters*, *196*(1-2), 17–33. https://doi.org/10.1016/S0012-821X(01)00588-X

Tomljenović, B., Csontos, L., Márton, E., & Márton, P. (2008). Tectonic evolution of the northwestern Internal Dinarides as constrained by structures and rotation of Medvednica Mountains, North Croatia. *Geological Society, London, Special Publications*, *298*(1), 145–167. https://doi.org/10.1144/SP298.8

Tremblay, A., Meshi, A., Deschamps, T., Goulet, F., & Goulet, N. (2015). The Vardar zone as a suture for the Mirdita ophiolites, Albania: Constraints from the structural analysis of the Korabi-Pelagonia zone. *Tectonics*, *34*, 352–375. https://doi.org/10.1002/2014TC003807

Trotet, F., Goffe, B., Vidal, O., & Jolivet, L. (2006). Evidence of retrograde Mg-carpholite in the Phyllite-Quartzite nappe of Peloponnese from thermobarometric modelisation-geodynamic implications. *Geodinamica Acta*, *19*(5), 323–343. https://doi.org/10.3166/ga.19.323-343

Ustaszewski, K., Kounov, A., Schmid, S. M., Schaltegger, U., Krenn, E., Frank, W., & Fügenschuh, B. (2010). Evolution of the Adria-Europe plate boundary in the northern Dinarides: From continent-continent collision to back-arc extension. *Tectonics*, *29*, TC6017. https://doi.org/10.1029/2010TC002668

Uunk, B., Brouwer, F., ter Voorde, M., & Wijbrans, J. (2018). Understanding phengite argon closure using single grain fusion age distributions in the Cycladic Blueschist Unit on Syros, Greece. *Earth and Planetary Science Letters*, *484*, 192–203. https://doi.org/10.1016/j.epsl.2017.12.031

van Hinsbergen, D. J., Dupont-Nivet, G., Nakov, R., Oud, K., & Panaiotu, C. (2008). No significant post-Eocene rotation of the Moesian Platform and Rhodope (Bulgaria): implications for the kinematic evolution of the Carpathian and Aegean arcs. *Earth and Planetary Science Letters*, *273*(3-4), 345–358. https://doi.org/10.1016/j.epsl.2008.06.051

Vidal, O., Goffé, B., & Theye, T. (1992). Experimental study of the stability of sudoite and magnesiocarpholite and calculation of a new petrogenetic grid for the system FeO–MgO–Al_2O_3–SiO_2–H_2O. *Journal of Metamorphic Geology*, *10*(5), 603–614. https://doi.org/10.1111/j.1525-1314.1992.tb00109.x

Vidal, O., & Theye, T. (1996). Petrology of Fe–Mg-carpholite-bearing metasediments from NE Oman. *Journal of Metamorphic Geology*, *14*(3), 381–397. https://doi.org/10.1111/j.1525-1314.1996.00381.x

Vidal, O., Theye, T., & Chopin, C. (1994). Experimental study of chloritoid stability at high pressure and various fO 2 conditions. *Contributions to Mineralogy and Petrology*, *118*(3), 256–270. https://doi.org/10.1007/BF00306647

Walcott, C. R. (1998). The alpine evolution of Thessaly (NW Greece) and late Tertiary Aegean kinematics, Utrecht University.

Warren, C. J., Hanke, F., & Kelley, S. P. (2012). When can muscovite 40Ar/39Ar dating constrain the timing of metamorphic exhumation? *Chemical Geology*, *291*, 79–86. https://doi.org/10.1016/j.chemgeo.2011.09.017

Whitney, D. L., & Evans, B. W. (2010). Abbreviations for names of rock-forming minerals. *American Mineralogist*, *95*(1), 185–187. https://doi.org/10.2138/am.2010.3371

Wijbrans, J., Pringle, M., Koppers, A., & Scheveers, R. (1995). Argon geochronology of small samples using the Vulkaan argon laserprobe, paper presented at Proceedings of the Royal Netherlands Academy of Arts and Sciences.

Wijbrans, J. R., Schliestedt, M., & York, D. (1990). Single grain argon laser probe dating of phengites from the blueschist to greenschist transition on Sifnos (Cyclades, Greece). *Contributions to Mineralogy and Petrology*, *104*(5), 582–593. https://doi.org/10.1007/BF00306666